Analytical and numerical validation of a model for flooding by saline carbonated water

Alvarez, A. C.; Blom, T.; Lambert, W. J.; Bruining, J.; Marchesin, D.

DOI
10.1016/j.petrol.2017.09.012

Publication date
2018

Document Version
Final published version

Published in
Journal of Petroleum Science and Engineering

Citation (APA)
Alvarez, A. C., Blom, T., Lambert, W. J., Bruining, J., & Marchesin, D. (2018). Analytical and numerical validation of a model for flooding by saline carbonated water. *Journal of Petroleum Science and Engineering*, *167*, 900-917. https://doi.org/10.1016/j.petrol.2017.09.012

Journal of Petroleum Science and Engineering 167 (2018) 900–917

Contents lists available at ScienceDirect

Journal of Petroleum Science and Engineering

journal homepage: www.elsevier.com/locate/petrol

Analytical and numerical validation of a model for flooding by saline carbonated water

A.C. Alvarez [a,**,1], T. Blom [b,2], W.J. Lambert [c,1], J. Bruining [b,*,2], D. Marchesin [a,3]

[a] Lab. of Fluid Dynamic, IMPA, Dona Castorina 110, Jardín Botánico, Río de Janeiro, Brazil
[b] TU Delft, Civil Engineering and Geosciences, Stevinweg 1, 2628 CE Delft, The Netherlands
[c] ICT-UNIFAL, BR 267, Km 533, Rodovia José Aurélio Vilela, 11.999, Brazil

ARTICLE INFO

Keywords:
Riemann problem
Waterflooding
Enhance oil recovery

ABSTRACT

It has been shown experimentally in the literature that for clayey formations, oil with polar components and an aqueous phase with divalent ions, a secondary waterflood with low salinity water composition improves oil recovery by some 5–20%. Our focus is on a less well known mechanism, i.e. low salinity enhanced solvent (e.g. carbonated water) recovery, as low salinity enhances the aqueous solubility of carbon dioxide. Indeed, after injection the latter is transferred from the aqueous to oleic phase thus decreasing the oil concentration in the oleic phase and diluting the residual oil. To study this mechanism we formulate the conservation equations of total hydrogen, oxygen, chloride and decane. Therefore, we solve analytically and numerically these equations in 1−D in order to elucidate the effects of the injection of low salinity carbonated water into a reservoir containing oil equilibrated with high salinity carbonated water. We use PHREEQC (acronym of pH-REdox-Equilibrium C-program) to obtain the accurate equilibrium partition of neutral species that are soluble both in the oleic and the aqueous phase by application of the Krichevsky-Ilinskaya extension of Henry's law for solubility of gases in liquids. Using Gibbs phase rule it can be shown that the phase behavior only depends on the pH and the chloride concentration. The above mentioned equilibrium relations use Pitzer's activity coefficients to extend the validity up to 6M. We obtain the saturation, composition and the total Darcy velocity profiles. The significant new insight obtained is that by changing only the salinity in carbonated waterflooding the oil recovery can be enhanced.

1. Introduction

Carbonated water flooding (Dong et al., 2011) increases oil production due to favorable dissolution effects, viscosity reduction (Welker et al., 1963) and bactericide effects, which enhance the injectivity (Christensen et al. (1961)). In De Nevers et al., (1964) an extended Buckley-Leverett model is proposed, with partition of CO_2 between the oleic phase and aqueous phase (see also Welge et al. (1961)). The viscosities and densities of the aqueous and oleic phases depend on the carbon dioxide concentration. The pressure is taken high enough to avoid the presence of gas. As opposed to the Buckley-Leverett profile (Buckley et al. (1942), Leverett et al. (1939)) the solution, from upstream to downstream, consists of a constant state, a shock, a saturation/concentration rarefaction wave, a constant state with zero carbon dioxide concentration followed by a rarefaction and then a shock. The presence of CO_2 increases the oil recovery. Pope (1980), in his celebrated paper, formulates the fractional flow theory for a carbonated water flood. He got an approximation for the solution by replacing the saturation/concentration rarefaction wave by a shock.

In Grogan et al. (1987) a model that includes molecular diffusion and indicates its importance in dead-end-pore recovery is proposed. In all of these studies, the effect of salt was not explicitly taken into account. Dong et al. (Dong et al., 2011), in their experimental study, mention the alteration to more water-wet conditions and reduction of the water-oil

* Corresponding author.
** Corresponding author.
E-mail addresses: meissa98@impa.br (A.C. Alvarez), H.P.W.Blom@student.tudelft.nl (T. Blom), wanderson.lambert@gmail.com (W.J. Lambert), J.Bruining@tudelft.nl (J. Bruining), marchesi@impa.br (D. Marchesin).

[1] This author's work was supported by CAPES/IMPA Portal.
[2] CAPES Nuffic-024/2011, Technical University of Delft, Section Petroleum Engineering.
[3] CNPq under Grants 402299/2012-4, 301564/2009-4, 470635/2012-6, FAPERJ under Grants E-26/111.416/2010, E-26/102.965/2011, E-26/110.658/2012, E-26/111.369/2012, E-26/110114.110/2013, ANP-731948/2010, PRH32–6000.0069459.11.4.

https://doi.org/10.1016/j.petrol.2017.09.012
Received 24 February 2017; Received in revised form 29 August 2017; Accepted 10 September 2017
Available online 15 September 2017
0920-4105/

interfacial tension as additional factors for improved oil recovery. Morrow et al., (2011) show that low salinity can indeed lead to enhanced recovery. Scott et al. (1965) mention bypassing as a reason for disappointing recovery in a carbonated flood field experiment. However, the first year, the K&S carbonated water flood (Hickok et al. 1960) produced in one year more oil than in the preceding 29 years of primary recovery. Part of the production came from watered out regions. Ramesh et al. (1973) developed a 2-D numerical model of a carbonated water flood.

A frequently mentioned effect of low salinity is improved relative permeability behavior. General observations are that in water-wet media, oil will occupy the larger pores and obstruct the flow of water, leading to low relative water-permeabilities. Low relative water permeability leads to a favorable mobility ratio and more stable displacement. However, residual oil saturations are lower in mixed wet media. All of this means that the advantage of increased water-wet behavior is not straightforward. The phase behavior plays an important role. We will use the decane-carbon dioxide system for reasons of clear illustration.

It is possible to combine some experimental data Reamer and Sage (1963), Nagarajan and Robinson (1986), but other experimental data (Kariznovi et al., 2013) do not smoothly connect to these data; this connection is achieved once we use the Krichevsky-Ilinskaya equation (Pope, 1980), an extension of Henry's law to parametrize the experimental data. It is possible to combine the equations for the oleic and aqueous phase to obtain the partition coefficient of carbon dioxide between the aqueous and oleic phase. The presence of electrolytes decreases the solubility of carbon dioxide in the aqueous phase (salting out effect), which is described by the Setchénow coefficient, (Randall and Failey, 1927a, 1927b, 1927c). We will use these expressions to quantify the effect of low salinity on carbonated water flooding.

In Sohrabi et al. (2009) the mechanisms of carbonated water injection (CWI) using micromodels are studied. They show that recovery in light oils mainly depends on the dissolution of CO_2 in the oil, whereas the enhancement of recovery of heavy oil is due mainly to viscosity reduction.

To study the effects of CO_2 injection with low salinity waterflooding we focus on a one dimensional incompressible flow model that describes two-phase flow and dissolution in phases based on geochemistry (Farajzadeh et al. (2012)). These processes are studied by means of a system of conservation laws for the transported quantities. Using this model we study the flow in a sandstone rock filled with an oleic phase that contains both oil (an alkane, e.g. decane) and dissolved carbon dioxide as well as an aqueous phase also equilibrated with CO_2. Since we consider mass transfer of carbon dioxide between oleic and aqueous phases and the partial molar volume of CO_2 differs between phases, the total Darcy velocity varies.

We also consider ions (H_2O, H^+, OH^-, CO_3^{2-}, HCO_3^-, Cl^-), leading to what we call the chloride ionic carbon dioxide-oil-water (CLICDOW) model. The most relevant aspects of the effect of ions on the recovery of oil are studied with this model of composition waves (Bryant et al., 1986, 1987; Helfferich, 1989; Lake, 1989; Lake et al., 2014). To illustrate these effects we inject water with the same *pH* but with lower salinity than the initial salinity in the core.

In this paper, we obtain analytically the Riemann solution, which consists basically in applying the method of characteristics (MOC). This method seeks analytical solutions of the CLICDOW Model similarly to the those treated in De Nevers et al., (1964); Welge et al. (1961); Buckley et al. (1942); Leverett et al. (1939); Pope (1980); Dumore et al. (1984); Helfferich et al. (1981); Johns et al. (1993). The Riemann solution consists in a concatenation of rarefaction and shock waves implementing certain admissibility conditions (Lax, 1957; Oleinik, 1957; Glimm, 1965; Liu, 1974, 1975).

A Riemann solver for the proposed geochemical model serves to quantify and explain how the geochemical processes of CO_2 with low salinity water injection in a carbonated reservoir improve the oil recovery. At the same time, if we assume the salinity as constant our model clarifies the discrepancy between the solutions proposed by De Nevers et al., (1964) and by Pope (1980).

A Riemann solver is developed to obtain the solutions for a compositional model. In this solver, we automate the construction of slow and fast solution paths. To do so, we take into account the bifurcation structures which are not part of the classical fractional flow method used by Pope (1980). We, also provide comparisons with numerical solutions obtained by means of a commercial program, which is useful for the verification of the analytical solutions.

In the CLICDOW model coefficients in the system of conservation laws are estimated by means of PHREEQC program (PHREEQC version 3 is a computer program written in C++ and is designed to perform a wide variety of aqueous geochemical calculations; see details about its implementation in Parkhurst and Appelo (2013), Parkhurst et al. (1999)). This procedure is extremely useful because allows to include in a unified manner the geochemistry, the equilibrium reactions and the charges balance. Also, the method employed is a robust recovery procedure that serves to study more complex situation as for example to include more chemical species in the system. In this way we reduce the mathematical complexity associated with considering the large number of physical constraints and parameters that are included in the Geochemistry PHREEQC program.

The motivations for writing this paper are (1) to introduce a new methodology based on the extended Gibbs phase rule as a way to incorporate geochemistry in oil recovery simulations, which circumvents simultaneous solution of the transport equations and equilibrium relations (2) to show the effect of high salt concentrations on oil recovery and (3) to analyse the wave structure of the solutions (e.g. the occurrence of a pH wave embedded in a constant pH flood). The Riemann solution confirms that a pH peak wave found numerically with various numerical schemes, inclusive discontinuous Galerkin, was indeed no numerical artefact. Moreover, we make plausible that the unstable numerical solutions at low pH <2.7 can be traced back to the high sensitivity of the compositions at these pH values.

The additional advantage of the Riemann solution is that it can be used to perform a bifurcation analysis, and to make an inventory of the possible qualitatively different solutions. The bifurcations occur at coincidence and inflection loci. Clearly, bifurcations are essential to build the analytical solution, as well as to determine the location where qualitative changes of the behavior of the solution are expected. This determination is useful tool of mathematical modeling of oil recovery.

By means of numerical and analytical methods, we aim in this paper at quantifying the recovery improvement when carbonated water equilibrated at low salinity is injected in a reservoir that contains carbonated brine in equilibrium with an oleic phase and carbon dioxide. After introduction, Section II gives the physical model and we derive the model equations. Section III describes the Riemann solver and the strategy to obtain the Riemann solution. Section IV gives the model results in terms of the pH, the chloride concentration, the water saturation and the total velocity. The calculation suggests that a low salinity carbonated water flood improves the recovery because it admits a high dissolved concentration of carbon dioxide. We end with some conclusions. Appendix A describes the chemical species and Gibb's rule. Appendix B, C and D describe the method of characteristics, the Rankine-Hugoniot locus and the bifurcation surfaces. Appendix E shows the Riemann solution strategy in the projected space (S_w, pH).

2. Physical model

We consider low salinity injection (0.01 $mol/liter$ NaCl, with CO_2 saturated at a $pH = 2.74$) into an inert rock (1D) filled with an oleic phase that contains both oil and dissolved carbon dioxide as well as a brine (0.3 $mol/liter$) phase also at $pH = 2.74$. Injection and initial fluids contain carbon dioxide, the ensuing ions and sodium chloride. The initial fluid also contains oil (decane). We assume chemical equilibrium in both the aqueous phase and the oleic phase and equilibrium of carbon dioxide

between phases. The ions and water are only present in the aqueous phase, decane is only present in the oleic phase. Dissolution of oil (decane) in the aqueous phase is disregarded. Only carbon dioxide can be present both in the oleic phase and the aqueous phase. The injected fluid has a high carbon dioxide content, specified by the injection pH and salt concentration. We assume that the flow is governed by Darcy's law (Lorentz, 1913; Muskat and Meres, 1936; Hubbert et al., 1956) extended to two phase (Honarpour et al., 1986) and conservation laws for chemical species (Appelo and Postma, 2004; Muskat and Meres, 1936). We consider one dimensional incompressible flow. The temperature is chosen to be 71.11^{o}C because for this temperature there exist many data in the literature for the decane carbon dioxide system. We take the pressure to be well above the pressure at which a gaseous phase can exist.

The unit of viscosity is Pa.s (1 cP (1 cP = 10-3 Pa s). We disregard the salinity dependence of the viscosity, because this is outside the scope of the mathematical emphasis in the paper.

The model simulates oil recovery when water with CO_2 is injected in an inert sandstone rock at high pressure and medium temperature. We consider only seven species viz. CO_3^{2-},CO_2, OH^-, H_2O, HCO_3^-, H^+, Cl^-. The rock is saturated with oil and water. The water contains dissolved solutes like ions and minerals. The carbon dioxide is dissolved in the aqueous and oleic phases; therefore there is mass transfer of carbon dioxide between phases: the partial molar volume of carbon dioxide differs between phases, thus a variable total Darcy velocity ensues.

There are five conservation laws, namely for total carbon, hydrogen, oxygen, chloride and decane. Each one consists of four terms, i.e. accumulation, convection, molecular diffusion and capillary diffusion. Recall that in the context of the Riemann solver we neglect diffusion and capillarity effects.

2.1. Model: Chloride Ionic Carbon Dioxide-Oil-Water(CLICDOW)

We derive the model equations from the conservation laws for total hydrogen, total oxygen, total chloride and total organic carbon. The conservation laws hold for the four lumped components (called master species) that do not convert into each other. As a result of the charge balance equation, which can be derived from the conservation laws we can choose four of these equations, viz. the total hydrogen (H(1)), the twice oxygen minus hydrogen equation (to eliminate the H_2O), the chloride ion equation and the total organic carbon (C(-4)) equation. The composition obtained with PHREEQC preserves the charge balance. The total molality of hydrogen can be expressed in terms of the other molalities $m_{a;j}$ as follows $m_{a;H(1)}[mol/kgwater] = m_{a;HCO_3} + m_{a;H} + m_{a;OH} + 2m_{a;H_2O}$. The total molality of oxygen is given by $m_{a;O(-2)}[mol/kgwater] = 2m_{a;CO_2} + 3m_{a;CO_3} + 3m_{a;HCO_3} + m_{a;OH} + m_{a;H_2O}$. Taking the difference$m_{a,O-H} = m_{a;H(1)} - 2m_{a;O(-2)}$, we obtain $m_{a;O-H} = m_{a;H} - m_{a;OH} - 4m_{a;CO_2} - 6m_{a;CO_3} - 5m_{a;HCO_3}$, an equation from which the H_2O been eliminated. We do not give the total carbon equation as it is already incorporated due to the conservation of charge. The total molar concentration in the aqueous phase is given by $m_{a;tot} = m_{a;CO2} + m_{a;CO_3} + m_{a;HCO_3} + m_{a;H} + m_{a;OH} + m_{a;H_2O} + m_{a;Cl^-}$ and we find the aqueous phase mole fractions $x_{a;i}$ as $x_{a;H(1)} = m_{a;H(1)}/m_{a;tot}$, $x_{a;O-H} = m_{a;O-H}/m_{a;tot}$, etc.

Using thermodynamical reasoning, it is possible to verify that the number of degrees of freedom is two (see Appendix A), which we choose as chloride concentration $[Cl^-]$ (Cl) and the hydrogen ion concentration $[H^+]$ ($pH = -log([H^+])$) in the aqueous phase and therefore also all mole fractions will be functions of these two concentrations. It is easier to choose chloride as variable since there is a single chloride compound, whereas sodium forms several compounds.

The molar concentrations of components j for the aqueous phase $\rho_{a;j}$ are the product of the molar phase density ρ_w times the mole fractions of component j and $\rho_{o;j}$ the molar concentration in the oleic phase. The master species equations include the total hydrogen, the total oxygen, the total chloride and the decane equation. The total hydrogen equation reads

$$\partial_t\left(\phi S_w \rho_{a,H(1)}\right) + \partial_x\left(u f_w \rho_{a,H(1)}\right) = 0, \tag{1}$$

The chloride equation reads

$$\partial_t\left(\phi S_w \rho_{a,Cl(-1)}\right) + \partial_x\left(u f_w \rho_{a,Cl(-1)}\right) = 0, \tag{2}$$

where $\rho_{a,Cl(-1)}$ is the molar concentration of the chloride ion in the aqueous phase (Appelo and Postma (2004)).

The hydrogen minus twice oxygen equation reads

$$\partial_t(\phi S_w \rho_{a,O-H}) + 4\partial_t\left(\phi S_o \rho_{o,CO_2}\right) + \partial_x\left(u f_w \rho_{a,O-H}\right) + 4\partial_x\left(u f_o \rho_{o,CO_2}\right) = 0. \tag{3}$$

The equation above represent a conservation of species that can be interconverted, like inorganic carbon in HCO_3, CO_2, $CO_3(-2)$; decane belongs to organic carbon, and is a special species. Therefore we distinguish the species hydrogen H, oxygen O, organic and inorganic C, chloride Cl and sodium Na. It is also possible to take linear combinations of species equations, such as twice oxygen minus hydrogen, which has the advantage of eliminating (dominating water) from the equation. Because the number of sodium ions equals the chloride ions, we can discard the sodium equation. Moreover, we can omit one species balance because we need to satisfy the charge balance. We choose for the species balance equations four conservation laws, viz. the hydrogen, twice the oxygen minus hydrogen, organic carbon and chloride, which can be solved for the pH, Cl, the total velocity u and the water saturation S_w.

For the total organic carbon we have

$$\partial_t\left(\phi S_o \rho_{o,C(-4)}\right) + \partial_x\left(u f_o \rho_{o,C(-4)}\right) = 0. \tag{4}$$

Initial conditions for all quantities X are given by

$$X = X_{init} + (1 - 0.5(1 + \tanh((x - 0.1)/0.05)))(X_{bound} - X_{init}), \tag{5}$$

where $pH_{init} = 2.74$, $Cl_{init} = 0.3[mol/liter]$, $Cl_{bound} = 0.01[mol/liter]$, $S_{init} = S_{wc} = 0.15$, $S_{bound} = 1 - S_{or} = 1.0$, and $u_{inj} = 10^{-5}[m/s]$.

The fractional flows for water and oil are saturation-dependent functions defined as follows. We denote $S_e = (S_w - S_{wc})/(1 - S_{wc})$, for $S_w \geq S_{wc}$ and $S_e = 0$ for $S_w < S_{wc}$;$k_{rw}(S_w) = s_e^{(2/\lambda+3)}$ and $k_{ro}(S_o) = (1 - S_e)^2(1 - S_e^{(2/\lambda+1)})$, $(S_o = 1 - S_w)$. The water viscosity is taken as $\mu_w = 0.001$ and the oil viscosity as $\mu_o = 0.002$ when they are constant; then we have the fractional flow functions for the aqueous and oleic phases

$$f_w(S_w) = \frac{k_{rw}(S_w)/\mu_w}{(k_{rw}(S_w)/\mu_w + k_{ro}(S_o)/\mu_o)}, \quad \text{and } f_o(S_w) = 1 - f_w(S_w). \tag{6}$$

where the water and oil permeabilities $k_{rw}(S_w)$ and $k_{ro}(S_o)$ are expressed in terms of their saturations; μ_w and μ_o are the viscosities of the aqueous and oleic phases. We disregard capillarity and diffusive effects. The fractional flow is shown in Fig. 1.

2.2. Relative permeability

Low water-wet end-point relative permeabilities are conducive to favorable mobility ratios. In this case the main production is largely characterized by pure oil-production after which only a small amount of oil is produced. The residual oil saturation is high and therefore the ultimate recovery from water-wet cores is relatively low. This is in contrast with intermediate wet-relative permeabilities, where after water-breakthrough a long tail of mixed oil/water production occurs. So recovery before water-breakthrough is less effective than the recovery from water wet-cores. After water breakthrough however, the ultimate recovery from mixed wet-cores is higher than from water-wet cores (see Hirasaki et al. (1996), Anderson et al. (1987)).

3. Riemann problem

The system of hyperbolic equations (1)–(4) for $\rho_{a,H(1)}$, $\rho_{a,O-H} = \rho_{a,H(1)} - 2\rho_{a,O(2)}, \rho_{o,CO_2}, \rho_{a,Cl(-1)}$ and decane $\rho_{a,C(-4)}$ disregarding the diffusion term is rewritten as:

$$\frac{\partial G(W)}{\partial t} + \frac{\partial u\widehat{F}(W)}{\partial x} = 0, \tag{7}$$

with $W = (S_w, pH, Cl)$. We have the accumulation $G = (G_1, G_2, G_3, G_4)$ and flux $F = u\widehat{F}$ with $\widehat{F} = (\widehat{F}_1, \widehat{F}_2, \widehat{F}_3, \widehat{F}_4)$ functions are

$$\widehat{F} = \left(f_w\rho_{a,H(1)}, \quad f_w\rho_{a,Cl(-1)}, \quad f_w\rho_{a,O-H} + 4f_o\rho_{o,CO_2}, \quad f_o\rho_{o,C(-4)}\right), \tag{8}$$

$$G = \varphi\left(S_w\rho_{a,H(1)}, \quad S_w\rho_{a,Cl(-1)}, \quad S_w\rho_{a,O-H} + 4S_o\rho_{o,CO_2}, \quad S_o\rho_{o,C(-4)}\right). \tag{9}$$

We are interested in the Riemann-Goursat problem associated to (7), that is the solution of these equations with piecewise constant initial data

$$\begin{cases} L = (Sw_L, pH_L, Cl_L, u_L) & \textbf{if} \quad x < 0, \\ R = (Sw_R, pH_R, Cl_R,) & \textbf{if} \quad x > 0. \end{cases} \tag{10}$$

We do not impose conditions on the variable u_R because it is obtained from the other variables together with the solution in the system.

We assume that the fluid is incompressible, but there is mass transfer between phases of the carbon dioxide and the partial molar volume differs between phases, thus a variable total Darcy velocity is not constant through the porous medium.

In this work the coefficient functions $\rho_{a,H(1)}, \rho_{a,O-H}, \rho_{o,CO_2}, \rho_{a,Cl(-1)}$ and $\rho_{a,C(-4)}$ are obtained through PHREEQC program. These coefficients depend on the variables (pH, Cl) only (see Appendix A). The partition of carbon dioxide between the aqueous and oleic phases is not covered in PHREEQC and needs to be separately implemented, which is included in Appendix A.

3.1. Solution

The solution of a Riemann problem is a sequence of constant states and self-similar elementary waves that are either rarefaction or shock waves. These waves suffer modification at a state on the bifurcation loci shown in Fig. D.9 and D.10 in Appendix D. Together with the bifurcations loci, we need *compatibility and entropy* conditions to select the unique (physical) solution.

To construct the Riemann solution, we obtain first the wave sequence in (S_w, pH, Cl), using combinations of rarefactions $\mathscr{R}_s$, $\mathscr{R}_\Delta$, $\mathscr{R}_{Cl}$ (see Appendix B) as well as shock waves $\mathscr{S}_s$, $\mathscr{S}_\Delta$ and $\mathscr{S}_{Cl}$ (see Appendix C) taking into account the coincidence surfaces together with the inflections loci I_{S_w}, I_Δ and I_{Cl}. From these waves, we construct the profiles $(s_w(\xi), \xi)$ and $(pH(\xi), \xi)$ with $\xi = x/t$ for a fixed t (see for example Figs. 4–6).

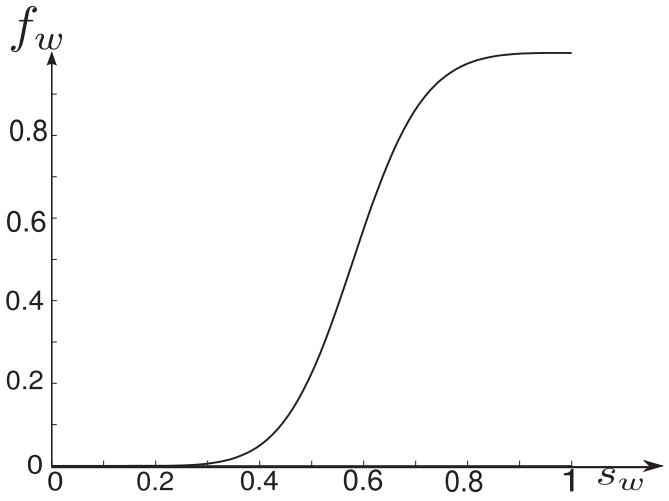

Fig. 1. Fractional flow f_w given by Eq. (6).

Since all waves must travel together there exists the natural restriction that if points in space state (S_w, pH, Cl) traverse from left to right in (x, t) space, then the characteristic velocity increases (at least non-decreases) along the Riemann solution, which is called *the geometrical compatibility* condition. This condition is used to select the physical sequence of waves for the Riemann solution. We denote by $\lambda_k(A)$, with $k = s, \Delta, Cl$ the characteristic velocity at state A and $\sigma(A, B)$ as the shock speed from state A to B.

For constructing the Riemann solution in a region where $\lambda_\Delta < \lambda_s < \lambda_{Cl}$, the geometrical compatibility condition requires that, we start with a composition rarefaction wave $\mathscr{R}_\Delta$, followed by either the constant state or a shock wave (see below), which can be either of the saturation or composition type and must have a velocity higher or equal than the previous wave. On the other hand, if $\lambda_{Cl} > \lambda_H > \lambda_s$, we start with a saturation wave $\mathscr{R}_s$ or S_s. Fulfilling the restriction due to the inflection curves and the admissibility conditions, we can initiate building the solution of the Riemann problem starting from the injection conditions of the reservoir (left state) until arriving at the initial conditions of the reservoir (right state).

An in-house Riemann solver was developed to represent wave curves which satisfy the compatibility and admissibility criteria. In this solver, we automate the construction of slow and fast solution paths taking into account the bifurcation structures. Taking these features into account is not easily done by the classical fractional flow method used by Pope (1980).

3.2. Strategy in the Riemann solver

In order to solve the Riemann-Goursat problem, we assume the *compatibility condition for the model* that the third component of the chemical composition wave $\mathscr{R}_\Delta$ is zero, i.e. $r^3_\Delta(S_w, pH, Cl) \equiv 0$ in equation (B.28). We can check that under the above condition the chemical composition wave R_Δ is invariant on the planes of constant Chloride concentration, $Cl = const$ in the projected space (S_w, pH, Cl). Also, we assume that the chloride wave curve S_{Cl} is transversal to the planes of constant chloride, $Cl = const$. These conditions are well fulfilled for the set of parameters obtained with PHREEQC program and they enable us to build the analytical solution. This fact is verified by numerical analysis of PHREEQC data.

The general procedure to solve the Riemann problem consists of the following steps: First we take waves along constant chloride planes, i.e. admissible rarefaction waves R_Δ, R_s, R_{Cl}, shock curves S_Δ, S_s, S_{Cl} or constant states. Secondly we use the auxiliary chloride waves R_{Cl} (which are contact waves i.e. characteristic speed is constant along the wave.), to go to other constant chloride planes corresponding to the right state.

For example, let us to construct the Riemann solution assuming that the left state $L = (Sw_L, pH_L, Cl_L)$ belongs to a region where the condition $\lambda_s < \lambda_\Delta < \lambda_{Cl}$ holds. Assuming the left and right belonging to distinct chloride planes i.e. $Cl_L \neq Cl_R$, the solution of the Riemann problem can be obtained with the following steps: First, from L to the state A where $\lambda_s(A) = \lambda_\Delta(A)$, we take a saturation wave $R_s(L)$ (See Fig. 2).

From this state, we take an admissible rarefaction $R_\Delta(A)$ connected to the physical boundary. Secondly, we continued this rarefaction waves $R_\Delta(A)$ by using an auxiliary transitional rarefaction chloride waves R_{Cl} and forming in this way an auxiliary surface (See Fig. 2). Here we use the fact that the waves R_{Cl} are contact, therefore the characteristic speed along this curve remains constant..

Subsequently, we take backward waves out of the right state $R = (Sw_R, pH_R, Cl_R)$, i.e. admissible rarefaction or shock waves on which the characteristic velocity decreases. Now we look for the intersection state C of the auxiliary surface with the backward curves $S_s(C)$ from C to

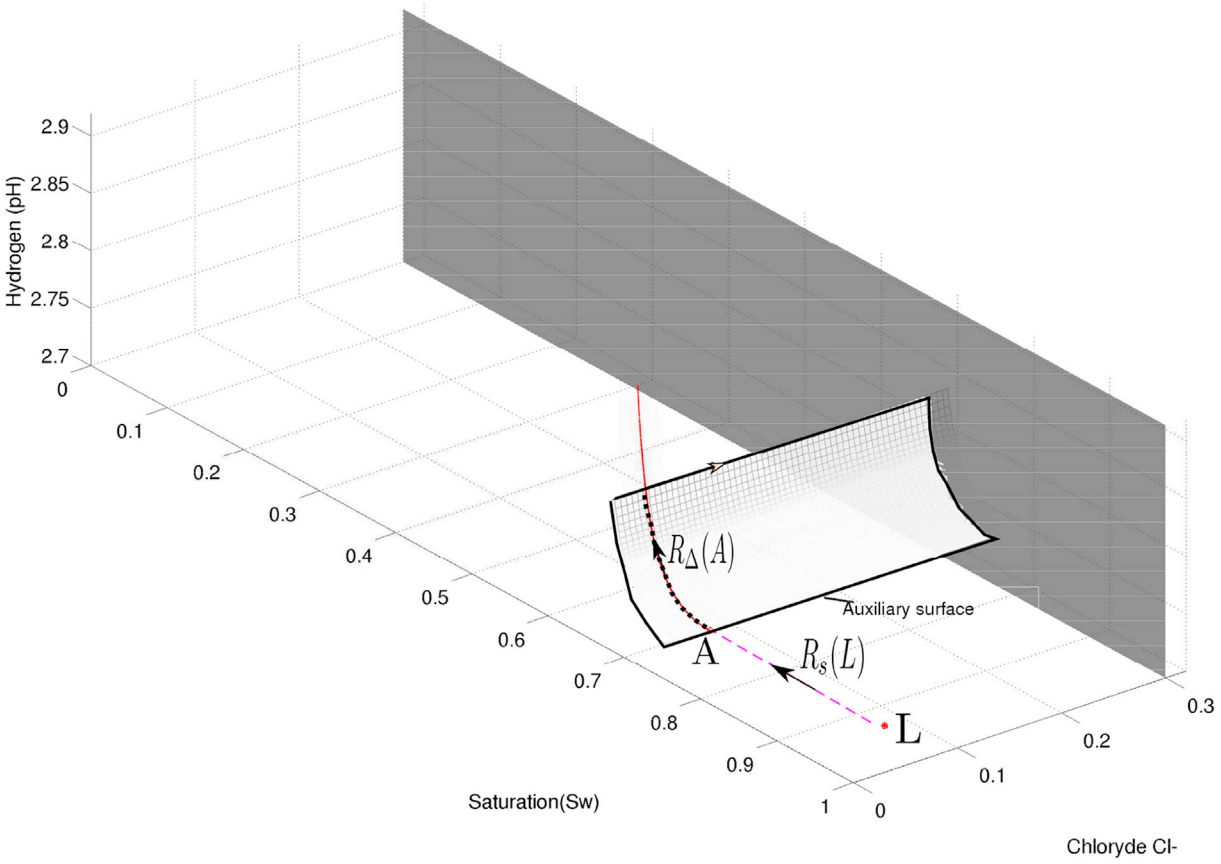

Fig. 2. Rarefaction saturation wave $R_s(L)$ connects the state L to the state A in which the characteristic speed coincides $\lambda_s(A) = \lambda_\Delta(A)$. From A, we take a rarefaction wave $R_\Delta(A)$. The auxiliary surface consists of a foliation with shocks $S_{Cl}(S)$, where S are initial states on $R_\Delta(A)$ in the plane of constant chloride $Cl = Cl_L$.

R (see Fig. 3). We check the geometrical compatibility condition at the point of intersection C, i.e. if the characteristic speed is smaller than or equal to the characteristic speed of the backward wave at the point of intersection C.

Fig. 3 shows the wave sequence satisfying the admissibility and geometric conditions for solving the Riemann problem for state left L and right state R used in this example.

The example described above shows a procedure to construct the wave sequence for a Riemann solution. In the general case, for any part of left and right states (in (10)) the procedure is similar, where one constructs the solution sequence in the projected space of variable S_w and pH and later in the full space (S_w, pH, Cl). We illustrate this procedure in Appendix E.

4. Analytical and numerical results

In this section we present the solution for an example relevant for oil recovery. We show the analytical solution from Riemann solver and the numerical schemes implemented in the commercial simulator COMSOL. COMSOL consists of a finite element solver and simulation software for various physics and engineering applications, especially coupled phenomena, or multiphysics, see www.comsol.com This comparison serves as verification for both solutions.

The in house developed Riemann solver can be used for verification in numerical solutions for compositional models. In this solver we utilized all the slow and fast solution paths in a unified manner allowing the discovery of structures that are not easily obtained by the classical fractional flow method.

The molar concentration coefficients obtained by PHREEQC are incorporated in multiphase flow simulation programmes, e.g. COMSOL and the Riemann solver, after applying a smoothing procedure for which we choose symbolic regression (EUREQA) (Eureqa is a modeling engine, which uses evolutionary search to determine regression equations that describe sets of data in their simplest form. www.nutonian.com/products/eureqa/). The COMSOL solver utilizes the method of finite elements to obtain the solution with an appropriate numerical diffusion to stabilize the solution.

Fig. 4 shows the profile of the chloride and hydrogen ion concentration for both the analytical solution obtained by the Riemann solver and the numerical method with COMSOL. It can be seen that the solutions agree extremely well and therefore the step function hydrogen solution obtained with COMSOL is not a numerical artifact for the convergence of the numerical solution.

Fig. 5 shows the water saturation profile corresponding to the Riemann problem solved here. There is also excellent agreement between the analytical and numerical solution. This profile shows a BL-type shock preceded by a constant state and a saturation of the chemical composition wave. In turn, these profiles show how the CLICDOW model is able to represent the mechanisms of enhanced oil recovery.

In this example, the solution consists of the following waves: from L to A, with $\lambda_s(A) = \lambda_\Delta(A)$, we take a rarefaction $R_s(L)$. From A to B we use a rarefaction $R_\Delta(L)$. But since we start with the same characteristic speed, the state A does not represent a constant state. From B to C, we take a shock $S_{Cl}(B)$ with speed $\sigma(B, C)$, which equals $\lambda_\Delta(A)$; therefore the state B does not represent a constant state. From C to R, we take a Buckley-Leverett shock $S_s(C)$. But the speed $\sigma(B, C) = \lambda_\Delta(B)$ is smaller than $\sigma(C, R)$; therefore the state C represents a constant state. This is because the self similar solution $U = (S_w(\xi), pH(\xi), Cl(\xi))$ with $\xi = x/t$ takes the same values between $\xi_1 = \lambda_\Delta(B)$ and $\xi_2 = \sigma(C, R)$ (Fig. 5 right). This constant state is shown in Fig. 5 left from $x = 3$ to $x = 4.3$ approximately. In summary, the solution is $R_s(L) \to R_\Delta(A) \to S_{Cl}(B) \to S_s(C)$, see in Fig. 3 left waves in phase state and the profiles $(S_w(\xi), pH(\xi), Cl(\xi))$ with $\xi = x/t$

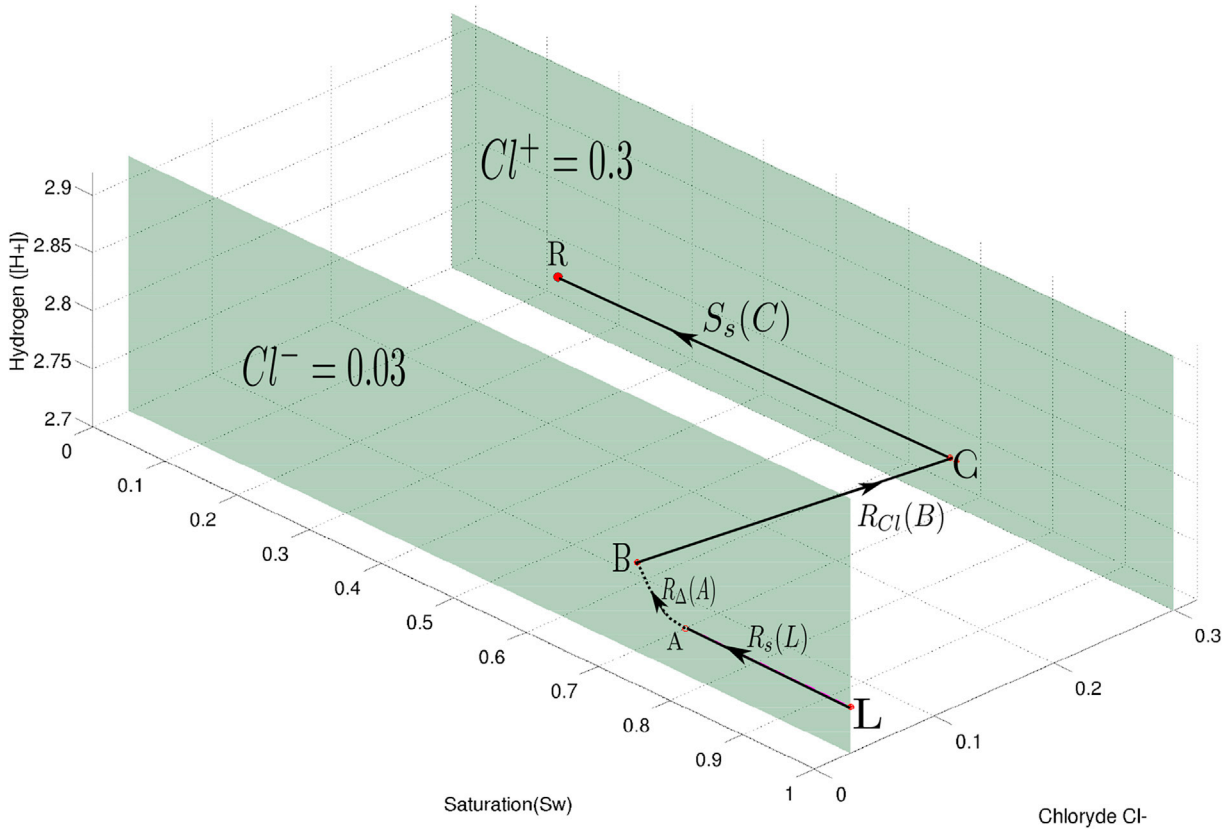

Fig. 3. Riemann solution corresponding to left (L) and right states (R). Solution is obtained as a concatenation of three wave curves separated by two constant states: the first consists of a rarefaction saturation wave $R_s(L)$ follows by a compatible rarefaction waves $R_\Delta(A)$, a second is an auxiliary rarefaction chloride waves $R_{Cl}(B)$ and a third is an admissible BL-shock $S_s(C)$.

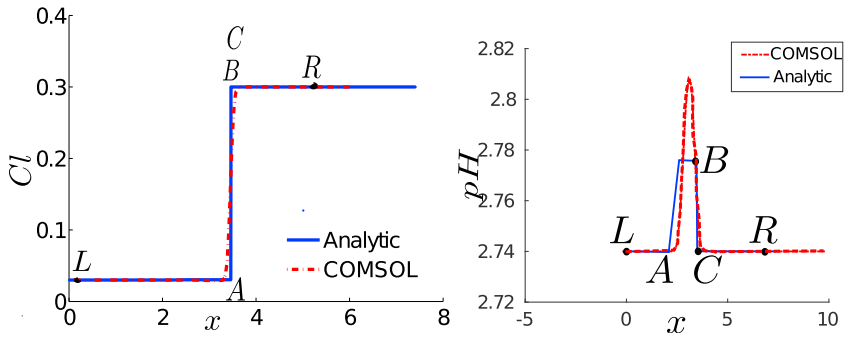

Fig. 4. Profile of chloride (left) and hydrogen (right) waves for analytical method (bold curve) and COMSOL (dashed curve) solution. We have excellent agreement for the chemical waves. The abscissa x-axis represents the value $\xi = x/t$ for $t = 10000$ sec.

in Figs. 4 and 5.

The constant solution appears on those state where the characteristic speeds and/or shock velocity does not coincide.

We attribute the mismatch between analytical and COMSOL solutions at $2 < x < 2.7$ to the fact that in this interval, we have a rarefaction wave R_Δ with characteristic speed close to the shock speed of S_Δ (almost a contact wave). Sometimes, this kind of wave is not easily captured by the numerical methods.

Fig. 6 plots the COMSOL solution of the water saturation and the chloride concentration as a function of distance at times (0.20000[s]) with intervals $\Delta t = 2000[s]$. The saturation (S_w) profile is similar to the Buckley-Leverett profile except that it shows a constant state between the Buckley-Leverett shock and the rarefaction wave. The chloride ($Cl^- := \rho_{a,Cl}$) profiles occur downstream of the rarefaction wave (Bryant et al., 1986, 1987, Helfferich, 1989; Lake, 1989).

Fig. 7 shows the COMSOL solution of the relative Darcy velocity u change, the saturation S_w, the chloride concentration Cl and the pH change versus distance for time (20000[s]). The advantage of the weak formulation option in COMSOL is that it does not require the addition of an artificial velocity accumulation term, e.g. $DTdu/dt$ term to obtain the total Darcy velocity profile.

Fig. 7 plots the weak formulation method results of the carbon dioxide concentration and decane concentration in the oleic phase. The figure shows that the low salinity injection gives an increased carbon dioxide concentration and a decreased decane concentration upstream leading to improved recovery.

In Fig. 8, we observe that the residual oil saturation consists of a fraction of ρ_{decane}/ρ_o of decane and by $1 - \rho_{decane}/\rho_o$ of CO_2. This implies that less oil is left behind as residual oil.

Figs. 4, 5 and 7 show the prevailing features of the numerical solution

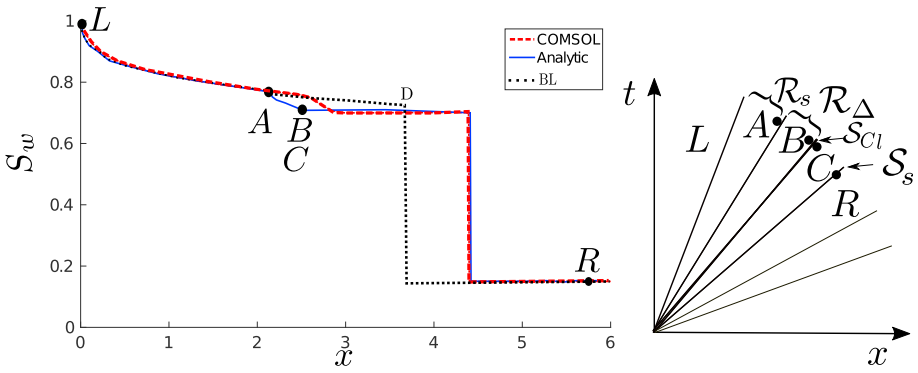

Fig. 5. (Left) Saturation profile for analytical method (bold curve) and COMSOL solution (dashed curve). We have good agreement between the solutions. Dotted line represents the Buckley-Leverett (BL) solution for a constant chloride concentration ($Cl = 0.3$). The abscissa x-axis represents the value $\xi = x/t$ for $t = 10000$ sec. (Right) Characteristic lines in the (x, t) plane with the corresponding admissible wave sequence.

obtained with COMSOL and the Riemann solver, which consists of three waves for similar injection and initial saturation conditions in Pope (1980). The hydrogen profile indicates that the pH starts to increase up to some state and then decreases forming a peak; meanwhile the water saturation decreases sharply and the pH and saturation move forward while the residual oil saturation decreases. Close to point of the abrupt change in pH, the chloride concentration forms a shock (contact wave) which is also transported in the water phase. Therefore, this shows that for these conditions the injection of CO_2 with brine improves oil recovery. The oil left behind after the passing of the shock is diluted with carbon dioxide, leading to a more favorable oil recovery. This fact together with the formation of the front with little residual oil explains the improvement in oil production. On the other hand, the increase of 5% in Darcy's velocity, also produces an increase in the speed of the shock with its corresponding positive effect on the recovery.

On the other hand, the efficiency of low salinity injection can be inferred in the following example. We assume that left (injection) and right (initial) state has the same chloride concentration $Cl = 0.3$ and $pH = 2.74$. In this case, the Riemann solution for $Sw_L = 1$ and $Sw_R = 0.15$ consists of the classical Buckley-Leverett solution, i.e. a rarefaction $R_s(L)$ to a state D, followed from D to R by a shock $S_s(A)$ such that $\lambda_s(D) = \sigma(D, R)$ (see Bucklet-Leverett (BL) solution in Fig. 5 right.). The BL shock amplitude is slightly greater than the low salinity (LS) shock amplitude, but the BL shock speed is much lower, so the oil recovery with (LS) is better.

The injected volume of the carbon dioxide saturated water is higher than the injected water only, which explains the fact that the area under the saturation curve is higher for carbon dioxide flooding.

When the salinity is constant, our model can be reduced to the model studied in De Nevers et al. (De Nevers et al., 1964), Pope (1980) by imposing similar injection and initial conditions. The structure of the Riemann solution in our example from left ($Sw_L = 1$, $pH_L = 2.7$) (upstream) to right ($Sw_R = 0.15$, $pH_L = 4$) (downstream) consists of two rarefaction waves connected by a chemical shock; the latter is continued with a constant state and finally a fast Buckley-Leverett saturation shock. In the first rarefaction wave only the saturation changes, while in the second one, both saturation and composition change. The connection point between the rarefaction waves can be constructed from a curve of states where the two characteristic velocities coincide.

In Pope (1980), the solution of the Riemann problem is obtained for constant viscosity oil as a sequence of a shock, a constant state, followed by another shock. Although we can only obtain a qualitative comparison with this solution because the author of Pope (1980) only presents a sketch, we can see from our sequence of waves of the Riemann solution that this solution differs from the one obtained in this paper with a similar initial

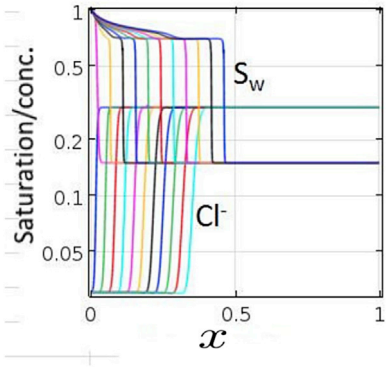

Fig. 6. Saturation and $Cl^- := \rho_{a,Cl}$ profiles. Initial and boundary $pH = 2.74$. Initial $Cl_{init} = 0.3[mol/liter]$ and $Cl_{bound} = 0.01[mol/liter]$ at the boundary. From left to right: $t = (0, 20000[s])$ with ïϵ $\Delta t = 2000[s]$. In this and all calculations below we use the porosity is $\varphi = 0.37$, $\mu_w = 1.0e-3[Pas]$, $\mu_o = 2.0e-3[Pas]$, $\lambda = 3$, $D_m = 1e-9[m^2/s]$, $D_{cap} = 1.0e-8[m^2/s]$.The x-axis represents dimensionless distance.

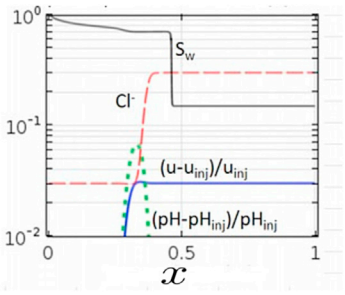

Fig. 7. Saturation wave, compositional waves and Darcy's velocity at $t = 10000[s]$. The x-axis represents dimensionless distance.

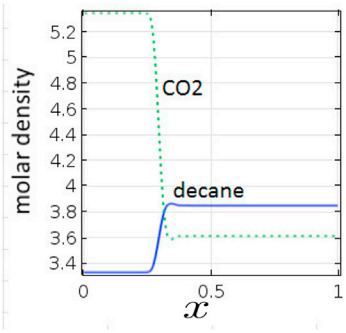

Fig. 8. Profiles of carbon dioxide and decane in dimensionless space. The x-axis represents dimensionless distance.

condition, which consists of a rarefaction, a constant state and a shock. We attribute the difference to the fact that the author uses a simplified model in which the total Darcy velocity is not allowed to change.

In De Nevers et al., (1964), a sketch of the appropriate solution of a similar Riemann problem is also presented. It consists of a wave sequence starting with the injection state, followed by a shock, a rarefaction and finally a shock, which is similar to ours. We attribute another cause for the difference between the solutions obtained in De Nevers et al. (De Nevers et al., 1964), Pope (1980) and those in the present paper to the sensitivity of the model to the flow f_w.

5. Conclusion

We developed a Riemann solver for oil recovery problems for low salinity carbonated waterflooding model including geochemical aspects. The methodology is adequate for one dimensional incompressible two-phase flow in porous media with a few chemical components.

Due to mass transfer between phases and a different partial molar volume of CO_2 in the aqueous and oleic phase, a variable Darcy velocity ensues. We quantify this change and we evaluated its contributions to the enhance oil recovery.

The performance of our Riemann solver is illustrated for carbonated water injection in a rock containing oil, brine water and carbon dioxide. We formulate four balance equations, in which we substitute expressions that are obtained from the geochemical software (PHREEQC) by regression.

There is acceptable agreement between the numerical solutions. This shows that the Riemann solver can effectively and accurately solve the injection problem for carbonated waterflooding with low salinity and elucidate the mechanism for enhancement of oil recovery.

Appendix

Appendix A. Chemical species and Gibbs' rule

As there is some arbitrariness in choosing the relevant aqueous species we follow Appelo et al. (2014) and Appelo and Postma (2004, 1999) and use the geochemistry program PHREEQC to analyze phenomena in the aqueous phase. PHREEQC makes a choice to disregard certain components, the concentrations of which are negligible. When we add water, carbon dioxide, salt and decane, there are eight different relevant chemical species, (Ns = 8), six that occur only in the aqueous phase, one, i.e. carbon dioxide, which occurs both in the aqueous phase and oleic phase and one alkane (decane), which occurs only in the oleic phase. The six species that occur in the aqueous phase have molal (Appelo and Postma (2004)) concentrations of species j and phase a, which is denoted by $m_{a,j}$, i.e. in *moles/kg* of solvent (water). The molality of carbon dioxide in the oleic phase is denoted by $m_{o;CO_2}$ [moles of component CO_2 per kg of decane]. The molality of decane in the oleic phase is denoted by $m_{o;dec} = 1$. There are three ($Nr = 3$) equilibrium reactions.

$$(CO_2)_{aq} + H_2O \rightleftharpoons HCO_3^- + H^+, \quad K_a = \frac{a_{a,HCO3}\, a_{a,H}}{a_{a,CO_2} a_{a,H_2O}}, \quad HCO_3^- \rightleftharpoons CO_3^{2-} + H^+, \quad K_b = \frac{a_{a,CO_3} a_{a,H}}{a_{a,HCO_3}}, \quad H_2O \rightleftharpoons OH^- + H^+, \quad K_w = \frac{a_{a,OH} a_{a,H}}{a_{a,H_2O}},$$

where $a_{a;j}$ [mol/kg-solvent] denotes the activity of molecule j in phase a; the reference state is an ideal solution with concentration of one molal. The activity is the product of the molality and the activity coefficient γ, i.e. $a_{a;j} = \gamma_{a;j} m_{a;j}$. The temperature dependent equilibrium constants can be found in the data bases of PHREEQC, e.g. phreeqc.dat or pitzer.dat. The choice of the data bases also determines how the activity coefficients will be calculated, phreeqc.dat selects the Debye-Hűckel expressions (Clarke and Glew, 1980; Fernandez et al., 1997), whereas pitzer.dat selects the Pitzer expressions Beyer and Staples (1986); Bradley and Pitzer (1979); Pitzer (1981, 1987); Pitzer and Mayorga (1973).

Appendix A.1. Gibbs phase rule

Gibbs phase rule to determine the number of chemical degrees of freedom consist in the following: Gibbs phase rule states Merkel et al. (2005) that the number of degrees of freedom N_f is given by $N_f = N_s - N_r - N_s + 2 - p$, where N_s is the number of different chemical species, N_r is the number of possible equilibrium reactions, N_c is the number of constraints, e.g. the charge balance. The number 2 represents the temperature and pressure and p the number of phases. Hence there are p equations of state (EOS). As we consider an aqueous and an oleic phase, the number of phases is $p = 2$. The charge balance equation acts as a constraint in Gibbs phase rule ($N_c = 1$). Because the charge balance equation can also be derived from the mass balance equations an alternative approach is to put $N_c = 0$, leading to one more degree of freedom for the composition dependence, but add an additional mass balance equation in Section IV (the total carbon equation). This is, however, less convenient, because then the composition depends on three instead of two variables.

If the relevant parameters are not tabulated, this is left to the user or default values for ideal solutions are used. The number of degrees of freedom can be calculated by $N_f = N_s - N_r - N_c + 2 - p = 8 - 3 - 1 + 2 - 2 = 4$. Given the pressure and temperature there are only two degrees of freedom for the composition variables, which we choose to be the $pH = -\log_{10}[a_{H+}]$ and the chloride concentration $[Cl^-]$. When the number of phases changes, the number of degrees of freedom for the compositions also changes (e.g. from a two phase system to a single phase system it increases by one). Therefore the total number of unknowns remains unchanged. In our examples we only consider the two-phase system.

In this way, we determine that we need only two chemically independent constituent of the system. Now we obtain the rest of the variables $[CO_2]$,$[H_2O]$,$[HCO_3]$,$[CO_3]$,[OH] in terms of pH and the chloride concentration $[Cl^-]$. Afterwards, we obtain relationships among the chemical species concentrations in terms of pH and Cl. At this point, we obtain a system in four dependent variables water saturation S_w, hydrogen concentration pH, chloride concentration Cl and Darcy's velocity u with four conservation laws (1)–(4). This procedure is justified from the physical point of view because the underlying model is fully described by the thermodynamics and conservation laws for chemical species. From the mathematical point of view, this means that we reduced a differential algebraic system (differential equations more constraints) to the differential system where the constraint are embedded into the coefficients, in which we solve the Riemann problem. In this paper, we focus on the solution of the differential system.

We use PHREEQC for the equilibrium calculations and chose 71.11 °C, because at this temperature the literature gives most data on the decane-CO2 system. The pH = 2.74 in our example and the corresponding pressure is 251 atm. A pressure of 136 atm close to 2000 psia would typically occur at a pH

of 2.86. In this pH range the solution is very sensitive to the pH values.

In the example studied here, we perform the estimation of the molar concentrations $\rho_{a,Cl(-1)}$, $\rho_{a,H+}$, $\rho_{a,O(2-)}$, $\rho_{o,C(-4)}$ in terms of pH and Cl by using first the PHREEQC program (Parkhurst and Appelo (2013), Parkhurst et al. (1999)) (Formulas for molar concentration are given in Section 2.1). We add some formulas to this program to obtain ρ_{o,CO_2} in terms of ρ_{a,CO_2} by using Henry's law. Secondly, we use a nonlinear regression package Eureqa.

The above method consists of the following steps: first, we assume as known the values of certain initial concentrations (pH_i), which we obtain from number of degrees of freedom determined by Gibbs rule, (e.g. hydrogen, chloride). Afterwards, using the Newton-Raphson procedure implemented in PHREEQC program, we obtain the concentration of other quantities. Using a non-linear regression we can obtain the concentrations of all the chemical species as function of two concentration variables.

PHREEQC program uses the values of the temperature dependent equilibrium coefficients of the equilibrium reactions for a preset temperature. Since a set of all master species transport equations implies the preservation of the charges, we use this equation (charge conservation) in the recovery procedure to reduce uncertainty. Also, we replace one combination of the mass conservation equations by the charge conservation. In the presence of the remaining mass conservation equations, the charge conservation is equivalent to the equation it replaces, The result is one extra constraint equation, which can be used to eliminate one of the unknown variables. We are left with a smaller set of PDEs for mass conservation, which is easier to solve.

Appendix A.2. Partition of CO_2 into aqueous and oleic phases

The partition of carbon dioxide between the aqueous and oleic phases is not covered in PHREEQC and needs to be separately implemented. It is, however, possible to add basic programs in PHREEQC that allow including the two-phase behavior. First, we formulate the underlying theory. The equilibrium between aqueous and oleic carbon dioxide can be represented by

$$(CO_2)_o \rightleftharpoons (CO_2)_{aq}.$$

The equilibrium relation will be obtained by using an extended Henry's law both for the aqueous CO_2 system and for the oleic CO_2 system, relating the fugacity of the gaseous carbon dioxide to the activities of carbon dioxide in the aqueous and oleic phase respectively. The extended Henry's law is formulated as the Krichevski-Ilinskaya equation, which contains two main coefficients. For the carbon dioxide-decane system, the coefficients are the oleic Henry constant and an activity coefficient described by a Margules expression (Poling et al., 2001). For the aqueous system the coefficients are the aqueous Henry constant and the Pitzer activity coefficient for carbon dioxide. To obtain the values of the coefficients for the carbon dioxide-decane system we use the experimental data by Nagarajan and Robinson Jr (Nagarajan and Robinson, 1986). It is not possible to smoothly connect these data to other experimental data (Chou et al. (1990), Cullick and Mathis (1984), Eustaquio-Rincón and Trejo (2001), Jennings and Schucker (1996), Kariznovi et al. (2013), Kukarni et al. (1974), Reamer and Sage, 1963), Shaver et al. (2001)), either because pressure and temperature conditions are different or because there is no smooth transition between the data. By comparing the Henry coefficient of carbon dioxide between the oleic phase and the gas phase to the Henry coefficient between the aqueous and the gas phase it is possible to derive the partition coefficient of carbon dioxide between the oleic phase and the aqueous phase. By extending Henry's law Poling et al. (2001), i.e. $p = Hx$, where the pressure p is replaced by the fugacity $f_{g;CO_2}$ and the mole fraction x by the activity of carbon dioxide in phase α, i.e. a_{α,CO_2} $(\alpha = a, o)$, we make it applicable for high pressures in the subcritical region and for concentrated solutions. We obtain for the aqueous phase $a_{a,CO_2} = \gamma_{\alpha,CO_2} x_{a,CO_2}$.

$$f_{g,CO_2} / \gamma_{a,CO_2} x_{a,CO_2} = H^H_{wg} \exp\left(\frac{v^{\infty}_{o,CO_2}}{RT}\left(P - P^s_1\right)\right), \tag{A.1}$$

The right side of Eq. (A.1) represents Henry's coefficient corrected for the high prevailing pressure. The symbol $v^{\infty}_{o,co2}$ denotes the partial molar volume in the aqueous phase and P^s_1 the saturation pressure at atmospheric conditions. For the oleic phase we obtain

$$\frac{f_{g,CO_2}}{x_{o,CO_2} \exp\left(\frac{A}{RT}(1 - x_{o,CO_2})^2\right)} = H^H_{wg} \exp\left(\frac{v^{\infty}_{o,CO_2}}{RT}\left(P - P^s_1\right)\right),$$

where the activity $\gamma_{o,CO_2} x_{o,CO_2}$ is obtained using Margules expression for the activity coefficient (Poling et al. (2001))

$$\gamma_{o,CO_2} \exp\left(\frac{A}{RT}(1 - x_{o,CO_2})^2\right).$$

We assume that the fugacities f_{g,CO_2} in equilibrium with the aqueous or oleic phase have been given the same values, which implies that we disregard the small amounts of water vapor and decane vapor in the gaseous phase. This allows us to eliminate f_{g,CO_2} from the two equations. The ratio of the activities of carbon dioxide in the aqueous phase and the oleic phase is therefore constant if pressure and temperature are constant. The consequence is that the mole fractions change as the activity coefficient γ_{a,CO_2} varies.

For carbon dioxide in the aqueous phase, Henry coefficients as a function of temperature are tabulated in Sander (1999), Zawisza and Malesinska (1981). Reference Sander (1999) gives the inverse Henry constant $k_H[M/atm]$, with $k_H = c_{a,CO_2}/P$, where c_{a,CO_2} is the concentration of carbon dioxide in the aqueous phase and

$$\ln\left(k_H / k^o_H\right) = -\Delta H_w / R(1/T - 1/T_o), \tag{A.2}$$

where for carbon dioxide dissolution in water we have $k^o_H = 34.0[mole/m3/atm]$ at temperature $T_o = 298.15[K]$ and $\Delta H_w/R = 2400[K]$ with R denotes the gas constant universal. Sometimes k_H is not called the inverse Henry constant (coefficient), but just the Henry coefficient. The positive value of $\Delta H_w/R$ arises as the Henry coefficient H^H_{w-g} gives the conversion of the dissolved phase to the gas phase and this reaction is endothermic. Conversion of k^H to H^H_{w-g} uses equation (A.2) at $T = 298.15$ and $T = 344.3K$, respectively, i.e. $H^H_{w-g} = (\rho_w[kg/m^3]/Mw[kg/mole])\ k_H(1/34.0)[atm/mole/m^3] =$

$1593.2atm$ and $H^H_{w-g} = (\rho_w[kg/m^3]/Mw[kg/mole])\ kH(1/100.0)[atm/mole/m^3] = 542.05.2atm$. For the tabulated values Sander (1999), the fugacity is equal to the low saturation pressure and this equality allows to determine H^H_{w-g} from the data. The activity coefficient γ_{a,CO_2} deviates noticeably from one only in ionic solutions and is only negligibly affected by neutral molecules. The activity coefficients of neutral molecules, such as $CO_2(aq)$, can be found in terms of the Setchénow coefficient (Randall and Failey, 1927a, 1927b, 1927c; Reardon and Langmuir, 1976; Byrne and Stoessell, 1982, Anderson and Crerar, 1993) use the Setchénov equation $\log_{10}\gamma_{a,CO_2} = \sum k_{Si}\mu_i := \mu k_S$, which takes into account the ionic species dependence, i.e. the ionic strength of species i:$\mu_i = m_{a,i}z_i^2/2$ with specific coefficient k_{Si} leading to an average Setchénow coefficient k_S at ionic strength $\mu = \sum \mu_i$.

For CO_2 in the oleic phase, we use the data set of Nagarajan and Robinson Jr (Nagarajan and Robinson, 1986), as it shows less scatter than other data sources and it reports both the compositions and the densities. Moreover, it gives data for a relevant temperature value, i.e. $T = 344.3K$. Unfortunately this dataset does not show any results for pressures below 63.85 bar. The data presented by other authors are not sufficiently complete to derive the behavior over the full concentration range. For this reason, we use again the Krichevsky-Ilinskaya equation (Poling et al. (2001)) to relate the carbon dioxide pressure in the gas phase to the concentration in the oleic phase. It is a relationship, which needs to be determined experimentally. Comparing to the data quoted in (Nagarajan and Robinson Jr (Nagarajan and Robinson, 1986)), we find for the decane-CO_2 system at $344.3K$ that $H^H_{o-g} = \exp(16.04)[Pa] = 91.25[atm]$ and $A = 2045.6[J/mol]$. The activity coefficient γ_{o,CO_2} corrects the mole fraction x_{o,CO_2} to the activity ao,CO_2.The value of A and the Henry coefficient were obtained by substituting experimental data of Nagarajan and Robinson Jr (Nagarajan and Robinson, 1986) in equation

$$x_{o,CO_2}\exp\left(\frac{A}{RT}(1-x_{o,CO_2})^2\right) = x_{a,CO_2}\gamma_{a,CO_2}\frac{H^H_{w-g}}{H^H_{o-g}}\exp\left(\frac{v^\infty_{a,co2}-v^\infty_{o,co2}}{RT}\left(P_o - P^s_1\right)\right). \tag{A.3}$$

Here $\Delta v = v^\infty_{a,co2} - v^\infty_{o,co2}$ is the difference between the partial molar volumes of carbon dioxide in the aqueous phase and in the oleic phase. The pressure P_o is chosen such that there is no gaseous phase, as CO_2 will dissolve in the oil, e.g. $P_o = 200\ bar$. The right side of Eq. (A.3), consists for a part of information on $a_{a,CO_2} = x_{a,CO_2}\gamma_{a,CO_2}$ that can be obtained with PHREEQC as a function of the pH and the chloride concentration and for a part from the Henry coefficients, and the partial molar volumes as explained above. The partial molar volumes of carbon dioxide in the oleic phase, (Nagarajan and Robinson Jr (Nagarajan and Robinson, 1986)) and the partial molar volume in the aqueous phase Parkhurst and Appelo (2013) are almost independent of the composition and thus constant. The difference of the partial molar volumes in the oleic and the aqueous phase must be attributed to the different effect of the carbon dioxide molecule on the volume of the mixture, see Israelachvili (2015) page 120. We used a data set at 71.11^oC, because at that temperature many measurements were obtained and reported in the literature. The Henry coefficient obtained from a linear regression shows the error of Henry's coefficient, i.e. $\ln H^H_{o-g} = 16.044 \pm 0.026$. Using this procedure we get a smooth transition between the measured high pressure data and the interpolated low pressure data. For the temperature used $T = 71.11^oC = 344.26K$ and use Equation (A.2) to obtain $ln(H^H_{o-g}) = 6.295$. The ratio $H^H_{w-g}/H^H_{o-g} = 5.940$. We use a system pressure of 200 bar to avoid the presence of gaseous CO_2, with respect to which the vapor pressure of water and decane are completely negligible, we obtain that $K_{eq} = H^H_{w-g}/H^H_{o-g}\exp\left(\frac{v^\infty_{a,co2}-v^\infty_{o,co2}}{RT}(P_0 - P^s_1)\right) = 4.396$.

We can use EUREQA to obtain an explicit expression for $x_{o;CO_2}$ of Eq. (A.3)

$$x_{o,CO_2} = 2.3061325\,\psi + 1.0883494\,\psi^2 \quad \& + 0.020187636\,exp\left(1.0576301\,\psi^2\right) - 0.020750111 - 2.4334976\,\psi\sqrt{\psi},$$

for which we denote the right side of Eq. (A.3) with ψ, which contains $a_{a,CO_2} = x_{a,CO_2}\gamma_{a,CO_2}$ and can be obtained with PHREEQC as a function of the pH.

The mole fraction of carbon dioxide in the oleic phase can be implemented in a BASIC routine appended to PHREEQC. This supplements the aqueous concentrations, which are conventionally obtained with PHREEQC (Appelo and Postma (1999), Appelo et al. (2014)). PHREEQC also gives the molar density of the aqueous phase as a function of the composition.

Appendix B. Method of Characteristic (MOC)

Appendix B.1. Rarefaction waves

We solve the Riemann-Goursat problem by the method of characteristics. To do so, we assume that the wave $W = (S_w, pH, Cl, u)$ are differentiable functions of the variable $\xi = x/t$, then $W(x,t) = W(x(\xi), t(\xi)) = W(\xi)$, and we obtain:

$$\left(-\xi\frac{\partial G}{\partial W} + \frac{\partial F}{\partial W}\right)\frac{\partial}{\partial \xi}(W) = 0. \tag{B.1}$$

The first eigenvalue is $\lambda_{S_w} = uf_w'/\phi$ associated to the eigenvector $\vec{r}_s = (1,0,0,0)^T$ (saturation wave $\mathscr{R}_{S_w}$) and the second (chemical composition wave $\mathscr{R}_\Delta$) is

$$\lambda_\Delta = (u/\phi)((f_w - (\Delta - 1))/(S_w - (\Delta - 1))),$$

associated to the eigenvector $\vec{r}_\Delta$ in. The third eigenvalue is $\lambda_{Cl} = (u/\phi)f_w/S_w$ which is a contact discontinuity (chloride wave $\mathscr{R}_{Cl}$) because $\nabla\lambda_{Cl}\cdot r_{Cl} = 0$, which is associated to the eigenvector $\vec{r}_{Cl}$. The saturation waves are curves with constant hydrogen (see Appendix B.2 for details).

Thus, we have three families of rarefaction waves, the saturation rarefaction, denoted by $\mathscr{R}_s$ and the chemical rarefactions, denoted by $\mathscr{R}_\Delta$ and $\mathscr{R}_{Cl}$. These waves are obtained as integral curves of each eigenpair, i.e. $d\mathscr{R}_s/d\xi = \vec{r}_s$ and $d\mathscr{R}_H/d\xi = \vec{r}_H$. To select the correct direction of the integral curve, we assume that the wave speed λ is increasing along of characteristic wave, which means that $\nabla\lambda\cdot\vec{r} > 0$ for each eigenpair. In the wave $\mathscr{R}_s$ only saturation changes and hydrogen and chloride concentrations remain constant; along such a wave the Darcy's velocity u is also constant. In this case, we have the classical Buckley-Leverett rarefaction wave.

The rarefaction $\mathscr{R}_\Delta$ is a composition wave in which the saturation, hydrogen, chloride concentrations and Darcy's velocity vary due to volume changes. This wave is obtained by integration of the complete first order differential system of equations (B.27)–(B.29), which is avoided in the fractional flow method as described in Pope (1980). For the rarefaction $\mathscr{R}_{Cl}$ mainly chloride and hydrogen concentrations change.

Appendix B.2. Method of characteristics. Technical calculation

MOC allows to calculate the velocity at which the waves propagate through the porous medium. The basis of the method is to assume that the independent variables $W = (S_w, pH, Cl, u)$ are functions of the variable $\xi = x/t$. Along any curve with tangent (dt, dx) we have

$$dW = \frac{\partial W}{\partial t}dt + \frac{\partial W}{\partial x}dx.$$

Using the system of conservation law (1)–(2), we obtain along characteristic curves for $i = 1, 2, 3$

$$\frac{\partial G_i}{\partial W}\frac{dW}{dt} + \frac{\partial F_i}{\partial W}\frac{dW}{dx} = 0, \tag{B.2}$$

where

$$\frac{\partial G_i}{\partial W} = \frac{\partial G_i}{\partial s_w}\frac{ds_w}{d\xi} + \frac{\partial G_i}{\partial y}\frac{dy}{d\xi} + \frac{\partial G_i}{\partial u}\frac{du}{d\xi}, \quad \frac{\partial F_i}{\partial W} = \frac{\partial F_i}{\partial s_w}\frac{ds_w}{d\xi} + \frac{\partial F_i}{\partial y}\frac{dy}{d\xi} + \frac{\partial F_i}{\partial u}\frac{du}{d\xi}.$$

In matrix notation equation (B.2) is

$$\left(-\xi\frac{\partial G}{\partial W} + \frac{\partial F}{\partial W}\right)\frac{dW}{\partial \xi} = 0, \tag{B.3}$$

where the accumulation and flux functions G are given in (8).

From now we rewrite above system of equations with another notation such that mathematical manipulation are more easily to do. Let us denote by $C_1 = \rho_{a,H(1)}$, $C_2 = 0$, $C_3 = \rho_{a,Cl(-1)}$, $C_4 = 4\rho_{o,CO_2}$, $C_5 = \rho_{a,O-H}$, $C_6 = \rho_{o,C(-4)}$ and $C_7 = 0$. We consider a system evolving chemical species $\theta = (\theta_1, \theta_2) = (pH, Cl)$, water saturation S_w and Darcy's velocity u. Molar concentrations are rewritten as $C_i = C_i(\theta)$, for $i = 1, \cdots, 7$ and the system of equations (1)–(2) can rewritten as:

$$\frac{\partial}{\partial t}(\phi S_w C_1) + \frac{\partial}{\partial x}(u f_w C_1) = 0, \tag{B.4}$$

$$\frac{\partial}{\partial t}(\phi(1-S_w)C_2 + S_w C_3) + \frac{\partial}{\partial x}u((1-f_w)C_2 + f_w C_3) = 0, \tag{B.5}$$

$$\frac{\partial}{\partial t}(\phi(1-S_w)C_4 + S_w C_5) + \frac{\partial}{\partial x}u((1-f_w)C_4 + f_w C_5) = 0 \tag{B.6}$$

$$\frac{\partial}{\partial t}(\phi(1-S_w)C_6 + S_w C_7) + \frac{\partial}{\partial x}u((1-f_w)C_6 + f_w C_7) = 0. \tag{B.7}$$

Notice that in the equations (B.4) and (B.7), we introduced $C_2 = 0$ and $C_7 = 0$ to ensure compatibility with system of equations (7)–(9).

Denoting $A = \frac{\partial F}{\partial U}$ and $B = \frac{\partial G}{\partial U}$, the system of eigenvalues is written as $A\vec{r} = B\lambda\vec{r}$, where $r = (S_w, \theta, u)^T$ and B, A:

$$B = \phi\begin{pmatrix} C_1 & S_w\frac{\partial C_1}{\partial \theta_1} & S_w\frac{\partial C_1}{\partial \theta_2} & 0 \\ C_3 - C_2 & (1-S_w)\frac{\partial C_2}{\partial \theta_1} + S_w\frac{\partial C_3}{\partial \theta_1} & (1-S_w)\frac{\partial C_2}{\partial \theta_2} + S_w\frac{\partial C_3}{\partial \theta_2} & 0 \\ C_5 - C_4 & (1-S_w)\frac{\partial C_4}{\partial \theta_1} + S_w\frac{\partial C_5}{\partial \theta_1} & (1-S_w)\frac{\partial C_4}{\partial \theta_2} + S_w\frac{\partial C_5}{\partial \theta_2} & 0 \\ C_7 - C_6 & (1-S_w)\frac{\partial C_6}{\partial \theta_1} + S_w\frac{\partial C_7}{\partial \theta_1} & (1-S_w)\frac{\partial C_6}{\partial \theta_2} + S_w\frac{\partial C_7}{\partial \theta_2} & 0 \end{pmatrix}, \tag{B.8}$$

$$A = \begin{pmatrix} uC_1\frac{\partial f_w}{\partial S_w} & uf\frac{\partial C_1}{\partial \theta_1} & uf_w\frac{\partial C_1}{\partial \theta_2} & \frac{\partial F_1}{\partial u} \\ u(C_3 - C_2)\frac{\partial f_w}{\partial S_w} & u(1-f_w)\frac{\partial C_2}{\partial \theta_1} + uf_w\frac{\partial C_3}{\partial \theta_1} & u(1-f_w)\frac{\partial C_2}{\partial \theta_2} + uf_w\frac{\partial C_3}{\partial \theta_2} & \frac{\partial F_2}{\partial u} \\ u(C_5 - C_4)\frac{\partial f_w}{\partial S_w} & u(1-f_w)\frac{\partial C_4}{\partial \theta_1} + uf_w\frac{\partial C_5}{\partial \theta_1} & u(1-f_w)\frac{\partial C_4}{\partial \theta_2} + uf_w\frac{\partial C_5}{\partial \theta_2} & \frac{\partial F_3}{\partial u} \\ u(C_7 - C_6)\frac{\partial f_w}{\partial S_w} & u(1-f_w)\frac{\partial C_6}{\partial \theta_1} + uf_w\frac{\partial C_7}{\partial \theta_1} & u(1-f_w)\frac{\partial C_6}{\partial \theta_2} + uf_w\frac{\partial C_7}{\partial \theta_2} & \frac{\partial F_4}{\partial u} \end{pmatrix}, \tag{B.9}$$

with $\frac{\partial F_1}{\partial u} = f_w C_1$, $\frac{\partial F_2}{\partial u} = (1-f_w)C_2 + f_w C_3$, $\frac{\partial F_3}{\partial u} = (1-f_w)C_4 + f_w C_5$ and $\frac{\partial F_4}{\partial u} = (1-f_w)C_6 + f_w C_7$. To obtain the eigenvalues we solve $det(A - \lambda B) = 0$, where $A - \lambda B$ is:

$$\begin{pmatrix} C_1\xi_1 & \xi_3\frac{\partial C_1}{\partial\theta_1} & \xi_3\frac{\partial C_1}{\partial\theta_2} & f_wC_1 \\ (C_3-C_2)\xi_1 & \xi_2\frac{\partial C_2}{\partial\theta_1}+\xi_3\frac{\partial C_3}{\partial\theta_1} & \xi_2\frac{\partial C_2}{\partial\theta_2}+\xi_3\frac{\partial C_3}{\partial\theta_2} & (1-f_w)C_2+f_wC_3 \\ (C_5-C_4)\xi_1 & \xi_2\frac{\partial C_4}{\partial\theta_1}+\xi_3\frac{\partial C_5}{\partial\theta_1} & \xi_2\frac{\partial C_4}{\partial\theta_2}+\xi_3\frac{\partial C_5}{\partial\theta_2} & (1-f_w)C_4+f_wC_5 \\ (C_7-C_6)\xi_1 & \xi_2\frac{\partial C_6}{\partial\theta_1}+\xi_3\frac{\partial C_7}{\partial\theta_1} & \xi_2\frac{\partial C_6}{\partial\theta_2}+\xi_3\frac{\partial C_7}{\partial\theta_2} & (1-f_w)C_6+f_wC_7 \end{pmatrix}. \tag{B.10}$$

where

$$\xi_1=\left(u\frac{\partial f_w}{\partial S_w}-\varphi\lambda\right),\quad \xi_2=u(1-f_w)-\varphi\lambda(1-S_w)\ \text{ and }\xi_3=uf_w-\varphi\lambda S_w. \tag{B.11}$$

After applying Gauss elimination procedure we obtain

$$\begin{pmatrix} C_1\xi_1 & \xi_3\frac{\partial C_1}{\partial\theta_1} & \xi_3\frac{\partial C_1}{\partial\theta_2} & fC_1 \\ 0 & \xi_3\eta_{21} & \xi_3\eta_{22} & 0 \\ 0 & \xi_3\chi_3+\xi_2\chi_1 & \xi_3\chi_4+\xi_2\chi_2 & 0 \\ 0 & \xi_3\eta_{41}-\xi_2C_1\frac{\partial C_6}{\partial\theta_1} & \xi_3\eta_{42}-\xi_2C_1\frac{\partial C_6}{\partial\theta_2} & -C_1C_6 \end{pmatrix}, \tag{B.12}$$

where

$$\eta_{ij}=-\frac{\partial C_1}{\partial\theta_j}(C_{2i-1}-C_{2i-2})+C_1\frac{\partial C_{2i-1}}{\partial\theta_j},\ \text{with}\quad i=1,\ldots,4; j=1,2.$$

$$\chi_1=C_1\left(C_4\frac{\partial C_6}{\partial\theta_1}-C_6\frac{\partial C_4}{\partial\theta_1}\right),\quad \chi_2=C_1\left(C_4\frac{\partial C_6}{\partial\theta_2}-C_6\frac{\partial C_4}{\partial\theta_2}\right), \tag{B.13}$$

$$\chi_3=C_6\eta_{31}-C_4\eta_{41}\quad \chi_4=C_6\eta_{32}-C_4\eta_{42}. \tag{B.14}$$

Then the first eigenvalue satisfies $\xi_1=0$ so we have

$$\lambda_s=(u/\phi)\frac{\partial f_w}{\partial S_w}, \tag{B.15}$$

associated to the saturation wave. One can prove that the eigenvector associated to this eigenvalue is $r_s=(1,0,0,0)$.

Second eigenvalue satisfies $\xi_3=0$, so we obtain

$$\lambda_{Cl}=(u/\phi)\frac{f_w}{S_w}. \tag{B.16}$$

This eigenvector $r_{Cl}=(r^1_{Cl},r^2_{Cl},r^3_{Cl},r^4_{Cl})$ associated to λ_{Cl} satisfies

$$\begin{pmatrix} C_1(\lambda_s-\lambda_{Cl}) & 0 & 0 & fC_1 \\ 0 & 0 & 0 & 0 \\ 0 & \xi_2\chi_1 & \xi_2\chi_2 & 0 \\ 0 & -\xi_2C_1\frac{\partial C_6}{\partial\theta_1} & -\xi_2C_1\frac{\partial C_6}{\partial\theta_2} & -C_1C_6 \end{pmatrix}\begin{pmatrix} r^1_{Cl} \\ r^2_{Cl} \\ r^3_{Cl} \\ r^4_{Cl} \end{pmatrix}=0. \tag{B.17}$$

Denoting $\widehat{\lambda}_s=(1/u)\lambda_s$ and $\widehat{\lambda}_{Cl}=(1/u)\lambda_{Cl}$ and solving system in (B.17) we obtain

$$\begin{aligned} r^1_{Cl} &= S_wf_w(f_w-S_w)\left(-\chi_1\frac{\partial C_6}{\partial\theta_2}+\chi_2\frac{\partial C_6}{\partial\theta_1}\right), \\ r^2_{Cl} &= \chi_2C_6\left(\widehat{\lambda}_s-\widehat{\lambda}_{Cl}\right), \\ r^3_{Cl} &= \chi_1C_6\left(\widehat{\lambda}_s-\widehat{\lambda}_{Cl}\right), \\ r^4_{Cl} &= -uS_w(f_w-S_w)\left(\widehat{\lambda}_s-\widehat{\lambda}_{Cl}\right)\left(-\chi_1\frac{\partial C_6}{\partial\theta_2}+\chi_2\frac{\partial C_6}{\partial\theta_1}\right), \end{aligned}$$

where χ_1 and χ_2 are given in (B.13). The third eigenvalue satisfies:

$$det\begin{pmatrix} \eta_{21} & \eta_{22} \\ \xi_3\chi_3 + \xi_2\chi_1 & \xi_3\chi_4 + \xi_2\chi_2 \end{pmatrix} = 0, \tag{B.18}$$

For this eigenvalue, we rewrite the integral curve parametrized by ξ in the plane *Cl* versus *pH*, i.e.

$$\frac{\frac{d\theta_1}{d\xi}}{\frac{d\theta_2}{d\xi}} = \frac{r^2_{Cl}}{r^3_{Cl}}, \tag{B.19}$$

where $\theta_1 = pH$ and $\theta_2 = Cl$. After some calculations, the equality $C_6/C_4 = constant$ holds.

For general case, we postulate that the eigenvalues have the form:

$$\lambda_\Delta = (u/\phi)\frac{(1-f_w)-\Delta}{(1-S_w)-\Delta}. \tag{B.20}$$

In fact, substituting λ_Δ given by (B.20) in ξ_2 and ξ_3, we obtain:

$$\xi_2 = u(1-f_w) - \phi\lambda(1-S_w) = -u\Delta\frac{(1-f_w)-(1-S_w)}{1-S_w-\Delta}. \tag{B.21}$$

and

$$\xi_3 = uf_w - \phi\lambda S_w = -u(1-\Delta)\frac{1-f_w-(1-S_w)}{1-S_w-\Delta}. \tag{B.22}$$

Substituting ξ_2 and ξ_3 in (B.18), after some calculations we obtain:

$$det\begin{pmatrix} \eta_{21} & \eta_{22} \\ (1-\Delta)\chi_3 + \Delta\chi_1 & (1-\Delta)\chi_4 + \Delta\chi_2 \end{pmatrix} = 0, \tag{B.23}$$

since we assume that $(1-f_w-(1-S_w))/(1-S_w-\Delta) \neq 0$. After some calculations we obtains

$$\Delta = \frac{\eta_{21}(C_6\eta_{31} - C_4\eta_{41}) - \eta_{22}(C_6\eta_{32} - C_4\eta_{42})}{\eta_{21}\chi_2 - \eta_{22}\chi_1 - (\eta_{21}(C_6\eta_{31} - C_4\eta_{41}) - \eta_{22}(C_6\eta_{32} - C_4\eta_{42}))}. \tag{B.24}$$

In particular, the eigenvalue λ_{Cl} in (B.16) is obtained taking $\Delta = 1$.

Denoting $\widehat{\lambda}_\Delta = (1/u)\lambda_\Delta$ the eigenvectors associated to λ_Δ can be found as:

$$\overrightarrow{r}_\Delta = \left((f_w - S_w)r_1, \quad (\widehat{\lambda}_s - \widehat{\lambda}_\Delta)r_2, \&(\widehat{\lambda}_s - \widehat{\lambda}_\Delta)r_3, \quad u(\widehat{\lambda}_s - \widehat{\lambda}_\Delta)(f_w - S_w)r_4\right),$$

where (r_2, r_3) are eigenvectors of matrix

$$\begin{pmatrix} \eta_{21} & \eta_{22} \\ (1-\Delta)\chi_3 + \Delta\chi_1 & (1-\Delta)\chi_4 + \Delta\chi_2 \end{pmatrix}, \tag{B.25}$$

moreover, $r_4 = \frac{f_w - S_w}{1-S_w-\Delta}\widehat{r}_4$, with

$$\widehat{r}_4 = \left(\sum_{i=1}^{2}\Delta(\eta_{4i}C_2 - \eta_{2i}C_4) + (1-\Delta)C_1\left(\frac{\partial C_4}{\partial\theta_i}C_2 - \frac{\partial C_3}{\partial\theta_i}C_4\right)\right),$$

and

$$r_1 = \frac{u\Delta}{1-S_w-\Delta}(\langle\nabla_\theta C_1, (r_2, r_3)\rangle + (1-f_w)C_1\widehat{r}_4),$$

here $\nabla_\theta C_1$ is the gradient of C_1 with respect to θ variable. The integral fields in the space θ do not depend on saturation.

The saturation waves are curves with constant hydrogen. The chemical composition curves ($i = \mathscr{R}_\Delta, \mathscr{R}_{Cl}$) can be obtained by solving first the differential equations

$$dS_w/d\xi = r_i^1\left((S_w, pH, Cl) = (f_w - S_w)r_1^i(pH, Cl),\right. \tag{B.26}$$

$$dpH/d\xi = r_i^2 S_w, pH, Cl) \tag{B.27}$$

$$dCl/d\xi = r_i^3(S_w, pH, Cl) = (\widehat{\lambda}_{S_w} - \widehat{\lambda}_\Delta)r_3^i(pH, Cl), \tag{B.28}$$

and secondly solving the ODE

$$du/d\xi = r_i^4(S_w, pH, Cl, u) = u(f_w - S_w)\left(\widehat{\lambda}_{S_w} - \widehat{\lambda}_\Delta\right) r_4^i(pH, Cl). \tag{B.29}$$

To select the correct direction of the integral curve, we assume that the wave speed λ is increasing along of characteristic wave, which means that $\nabla\lambda \cdot \overrightarrow{r} > 0$ for each eigenpair.

The integration (B.27)-(B.29) is avoided in the fractional flow method as described in Pope (1980). If we approximate our model by one in which no volume change on mixing occurs, the Darcy velocity is uniform in space and the method of characteristics can be fully applied as in Orr (2007)

Appendix C. Rankine-Hugoniot curve

Another type of solution are shock waves, which represent discontinuities. In phase space (s_w, pH, Cl, u) these discontinuity curves form the Rankine-Hugoniot locus (RH-locus). For a given left state (s_w^-, pH^-, Cl^-, u^-), the RH-locus is the set of right states (s_w^+, pH^+, Cl^+, u^+) that satisfy the Rankine-Hugoniot *RH* relationships

$$\sigma\left(G_i\left(s_w^+, pH^+, Cl^+\right) - G_i\left(s_w^-, pH^-, Cl^-\right)\right) =$$

$$u^+ \widehat{F}_i\left(s_w^+, pH^+, Cl^+\right) - u^- \widehat{F}_i\left(s_w^-, pH^-, Cl^-\right), \tag{C.1}$$

with $i = 1, 2, 3, 4$. Here $\widehat{F_1}$, $\widehat{F_2}$, $\widehat{F_3}$ and $\widehat{F_4}$ are given in (8) and G_1, G_2, G_3 and G_4 are given in (9) and the function σ represents the shock speed. In Lambert and Marchesin (2009), the authors obtain the RH-locus in space variables saturation, hydrogen concentration and chloride and then the RH-locus in the whole space (s_w, pH, Cl, u) is calculated.

Thus the Hugoniot locus is the union of three branches, i.e. $\mathscr{S}_s \cup \mathscr{S}_{H_1} \cup \mathscr{S}_{H_2}$, with

$$\mathscr{S}_s = \left\{\left(S_w^+, Cl^+, pH^+\right) : Cl^+ - Cl^- = 0, \text{and} \;\; pH^+ - pH^- = 0\right\}. \tag{C.2}$$

Along this branch we have that $u = u^+ = u^-$ and $\sigma = u[\widehat{F}_i]/[G_i]$, with $i = 1, 2, 3, 4$. Thus we call this curve a Buckley Leverett shock, in which only saturation varies. And the another two branches $\mathscr{S}_{H_1}$ and $\mathscr{S}_{H_2}$ consist of the intersection of two surfaces given in (C.3) and (C.4).

From (C.1) a sufficient condition for the existence of a non-trivial solution u^+, u^- and σ for (C.1) is that the following determinant conditions be satisfied in a region

$$H_1\left(S_w^+, pH^+, Cl^+\right) = det\begin{vmatrix} -\left[\widehat{F_1}\right] & \widehat{F_1}^- & [G_1] \\ -\left[\widehat{F_2}\right] & \widehat{F_2}^- & [G_2] \\ -\left[\widehat{F_3}\right] & \widehat{F_3}^- & [G_3] \end{vmatrix} = 0, \tag{C.3}$$

and

$$H_2\left(S_w^+, pH^+, Cl^+\right) = det\begin{vmatrix} -\left[\widehat{F_1}\right] & \widehat{F_1}^- & [G_1] \\ -\left[\widehat{F_2}\right] & \widehat{F_2}^- & [G_2] \\ -\left[\widehat{F_4}\right] & \widehat{F_4}^- & [G_4] \end{vmatrix} = 0. \tag{C.4}$$

This is a nonlinear system of equations in the variables S_w^+, pH^+ and Cl^+ for a fixed left state. The curve found in (S_w^+, pH^+, Cl^+) space gives the possible discontinuities that satisfy the shock conditions.

Since equations (C.3) and (C.4) determine the locus of two surfaces, their intersection (or Hugoniot locus) is a curve in three dimensional space determined by the variables (S_w^+, pH^+, Cl^+). Assuming the flux and accumulation are differentiable to order one, one can verify that the functions H_1 and H_2 in equations (C.3) and (C.4) can be decomposed into

$$H_i = \left(Cl^+ - Cl^-\right) SH_i^1\left(S_w^+, pH^+, Cl^+\right) + \left(pH^+ - pH^-\right) SH_i^2\left(S_w^+, pH^+, Cl^+\right),$$

with $SH_i^j(S_w^-, pH^-, Cl^-) \neq 0$ for $(i, j = 1, 2)$. The result above is obtained using Taylor's Series for H_1 and H_2 and the facts

$$H_1\left(S_w^-, Cl^-, pH^-\right) = 0, H_2\left(S_w^-, pH^-, Cl^-\right) = 0,$$

$$\frac{\partial H_1}{\partial s_w}\left(S_w^-, pH^-, Cl^-\right) = 0, \text{and} \;\; \frac{\partial H_2}{\partial s_w}\left(S_w^-, pH^-, Cl^-\right) = 0$$

hold.

Appendix D. Bifurcation surfaces

In this section, we present the coincidence and inflection loci, which are used to construct the Riemann solution, and to determine the *bifurcation*

surfaces where qualitative changes of the behavior of the solution are expected. Rarefaction wave solutions of the Riemann problem can suffer structural modifications along the loci where wave velocities coincide, i.e. *coincidence loci.* Here the coincidence are surfaces satisfying

$$\mathscr{C}_{s\Delta} = \{\lambda_s = \lambda_\Delta\}, \quad \mathscr{C}_{Cl\Delta} = \{\lambda_{Cl} = \lambda_\Delta\} \quad \mathscr{C}_{sCl} = \{\lambda_s = \lambda_{Cl}\}. \tag{D.1}$$

When the quantities S_w, pH and Cl vary, we have a coincidence surface. Let us denote $\mathscr{C} = \{(s_w, pH, Cl, u),$ such that $f_w = S_w\}$. One can prove that $\mathscr{C}_{sCl} = \mathscr{C}$. Choosing certain experimental data of interest obtained with the PHREEQC program, the coincidence surface in the projected space for fixed u consists of the following: For the data studied here the surface $\lambda_s = \lambda_\Delta$ consists of two surfaces close to the part of the planes $S_w = 0.41$ and $S_w = 0.76$ inside the physical domain, (See Fig. D.9). Similarly, the locus $\lambda_{Cl} = \lambda_\Delta$ consists of the plane $S_w = 1$ and another surface which is close to the plane $S_w = 0.60$. The coincidence surface $\lambda_s = \lambda_{Cl}$ consists of region of the physical domain close to the planes $S_w = 0.15$ and $S_w = 0.7371$. A fundamental feature of all coincidence surfaces is that they do not intersect each other for the data set studied here (see Fig. D.9). Besides, notice that we verify that coincidence surface $\lambda_s = \lambda_\Delta$ is included in the inflection surface associated to the wave $\mathscr{R}_\Delta$, as was pointed out theoretically in Helmut, 2011).

On inflection surfaces genuine nonlinearity is not satisfied (Lax, 1957), so we define the inflection locus for saturation waves and for composition waves as:

$$I_k = \left\{ W : \nabla\lambda_k \cdot r_k = \frac{l_k \cdot \left(r_k^t \frac{\partial^2 F}{\partial W^2} r_k - \lambda_k r_k^t \frac{\partial^2 G}{\partial W^2} r_k \right)}{(l_k \cdot B r_k)} = 0 \right\}, \tag{D.2}$$

with $W = (s_w, pH, Cl, u)$, with either $k = s, \Delta$ or Cl. Here B is the Jacobian of the accumulation G and $\frac{\partial^2 F}{\partial W^2}$, $\frac{\partial^2 G}{\partial W^2}$ denote the Hessian of accumulation and flux, respectively. We denote by r_k and l_k the right and left generalized eigenvectors of the matrix in (B.1), respectively (Helmut, 2011).

The role of inflection surfaces is to indicate where the corresponding family of rarefaction curves stop. One can check that in the projected state space (S_w, pH, Cl) the inflection surface for the saturation wave consists of the physical domain intersecting the plane

$$\mathscr{I}_s = \left\{ (S_w, pH, Cl) : \frac{\partial f_w}{\partial S_w} = 0 \right\}, \tag{D.3}$$

In our case, $\mathscr{I}_s$ corresponds approximately to the region $\{(S_w, pH, Cl) : S_w = 0.5791; 2.7 \leq pH \leq 3; 0.01 \leq Cl \leq 0.3\}$. Moreover, the inflection locus for the field R_Δ, denoted by $\mathscr{I}_\Delta$, is given by:

$$\mathscr{I}_\Delta = \mathscr{C}_{sCl} \cup \mathscr{C}_{s\Delta}, \tag{D.4}$$

The field $\mathscr{R}_{Cl}$ is linearly degenerated, in this case rarefactions and shocks coincide, i.e. $\mathscr{R}_{Cl} = \mathscr{S}_{Cl}$ and the wave speed is constant. We show the inflection surface in Fig. D.10. Riemann solution requires the characterization of the position and of features in the bifurcation surface. The bifurcation structures are almost parallel to the plane of constant saturation, i.e. the changes occurs on the direction S_w. One can check that in the projected state space (S_w, pH, Cl) the inflection surface for the saturation wave consists of the physical domain intersecting the plane given in (D.2). In our case, this surface corresponds approximately to the region $\{(s, pH, Cl) : s = 0.5791; 2.7 \leq pH \leq 3; 0.01 \leq Cl \leq 0.3\}$ (see Fig. D.10).

Appendix E. Riemann solution strategy in the projected space (S_w, pH)

In this appendix, we describe the Riemann solution (RS) in the projected space of variable S_w and pH. With this solution we construct the RS in the full space (S_w, pH, C, u). In this way, we show the wave curve method satisfying the geometry compatibility condition more clearly.

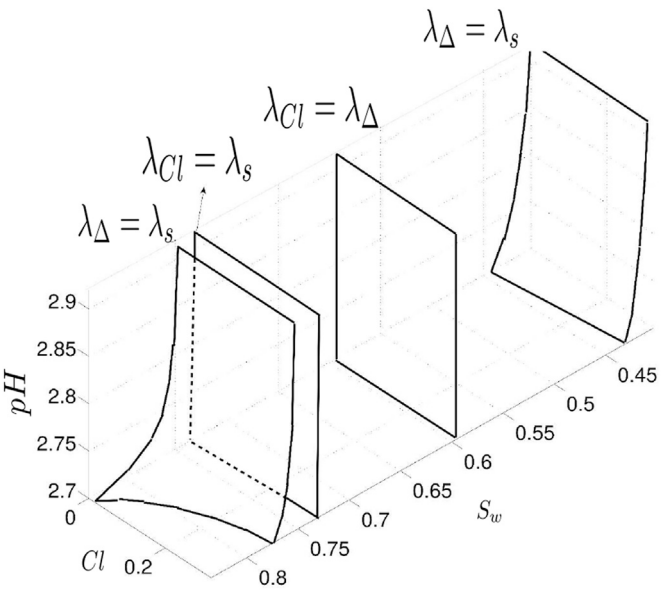

Fig. D.9. Coincidence Surfaces $\lambda_\Delta = \lambda_s$, $\lambda_{Cl} = \lambda_s$ and $\lambda_{Cl} = \lambda_\Delta$. These surfaces have almost constant saturation. It is expected that across the coincidence surface the structure of the Riemann solution changes.

When we seek the Riemann solution using a wave sequence fulfilling the geometric compatibility condition in a four-dimensional space (Sw, pH, Cl, u) the evaluation of many possibilities are required, resulting in a practically intractable method. However, combining geometric compatibility with the *compatibility condition for the model* described in Section 3.2, we can obtain a practically tractable method. With the compatibility condition for the model the waves $\mathscr{R}_s$, $\mathscr{R}_\Delta$, $\mathscr{S}_s$ and $\mathscr{S}_\Delta$ belong to the constant chloride plane. i.e. $Cl = constant$. Moreover, the waves $\mathscr{R}_{Cl}$ and $\mathscr{S}_{Cl}$ are transversal to planes $Cl = constant$ while maintaining the same characteristic velocity. These properties allow to develop the following procedure for constructing the Riemann solution:

(I) We consider Riemann data as in 10, i.e. with the form $L = (Sw_L, pH_L, Cl_L, u_L)$ and $R = (Sw_R, pH_R, Cl_R, u_R)$. We project data on two different planes: (Sw, pH)-plane, which we denote by $\tilde{L}$ and $\tilde{R}$ (see Figs. E.11 and E.12 left) and the (Cl, pH)-plane, which we denote by $\widehat{L}$ and $\widehat{R}$ (see Figs E.11 and E.12 right). There is no bifurcation projection on the (Cl, pH)-plane; in this projection the system is strictly hyperbolic. The field associated to λ_Δ is genuinely non-linear and the field associated to λ_{Cl} is linearly degenerated. We can use the classical theory of Lax to obtain the wave sequence in this projected plane.

(II) We obtain the Riemann solution connecting $\tilde{L}$ and $\tilde{R}$ in the (S_w, pH)-plane (we denote this wave sequence as $\mathbb{K}_1$), and the solution connecting $\widehat{L}$ and $\widehat{R}$ in the (Cl, pH)-plane (we denote this wave sequence as $\mathbb{K}_2$).

Once we have sequences $\mathbb{K}_1$ and $\mathbb{K}_2$, we compare both wave se-

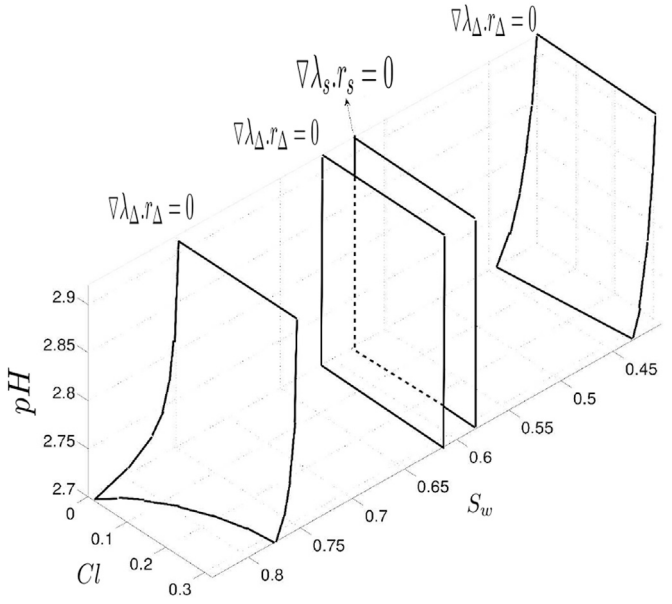

Fig. D.10. Inflection surfaces depend on eigenvalues $\nabla\lambda_\Delta \cdot r_\Delta = 0$ and $\nabla\lambda_s \cdot r_s = 0$. These surfaces have almost constant saturation S_w. Waves $\mathscr{R}_\Delta$ and $\mathscr{R}_s$ stop at the inflection locus.

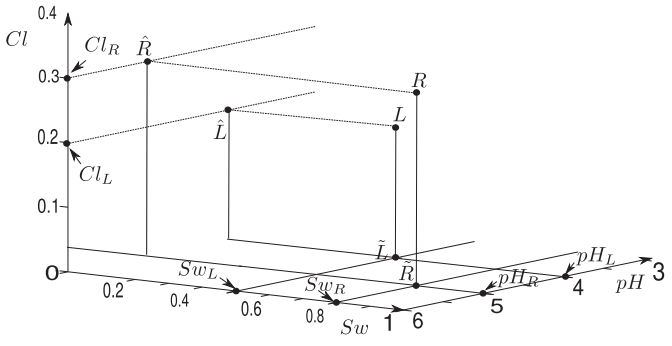

Fig. E.11. Projection of L and R data into (Sw, pH) and (Cl, pH) planes.

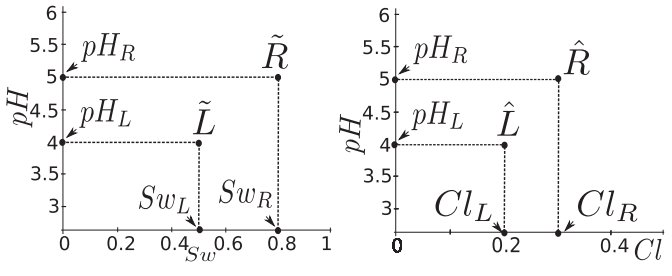

Fig. E.12. *a)- left.* Projection of L and R on (Sw, pH) plane, projections are denoted as $\tilde{L}$ and $\tilde{R}$, respectively. *b)- right.* Projection of L and R on (Cl, pH) plane, projections are denoted as $\hat{L}$ and $\hat{R}$, respectively.

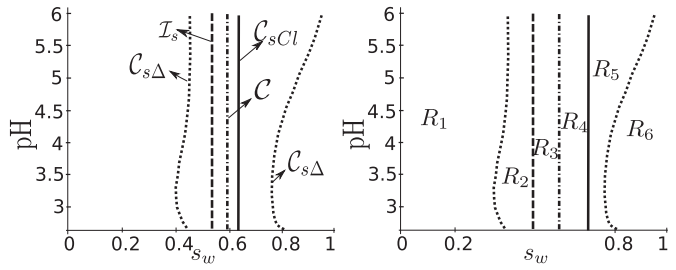

Fig. E.13. *a)- left.* Projection in the (S_w, pH) plane of coincidence and inflection surfaces described in Appendix D. Here $\mathscr{C} = \{(s_w, pH, Cl, u),$ such that $f_w = S_w\}$, while $\mathscr{C}_{s\Delta}$, $\mathscr{C}_{Cl\Delta}$ and $\mathscr{C}_{sCl}$ appear in (D.1). The inflection surface $\mathscr{I}_s$ is defined in (D.3). *b)- right.* Regions in the (S_w, pH) plane defined by coincidence and inflection surfaces. Here curves are out of scale such that we are able to define regions R_1 to R_6 in the same figure.

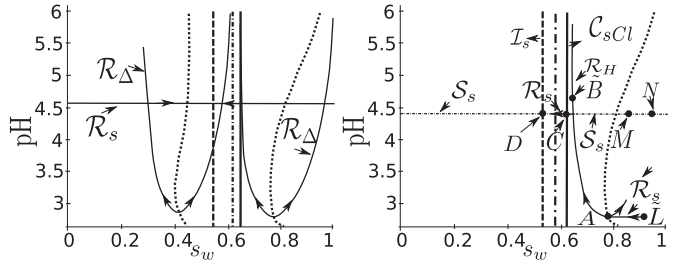

Fig. E.14. *a)- left.* Rarefactions $\mathscr{R}_\Delta$ and $\mathscr{R}_s$; arrows indicate the direction of increasing speed for each family. *b)- right.* The Riemann solution described in (1).

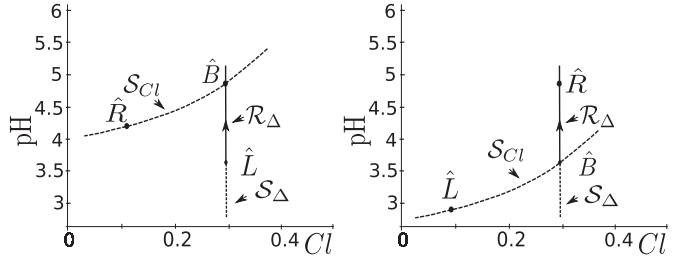

Fig. E.15. *a)- left.* Curves projected in (Cl, pH) plane. The vertical black line corresponds to $\mathscr{R}_\Delta$ and the arrow indicates the increasing of wave speed, the dashed part of vertical line is $\mathscr{I}_\Delta$. The diagonal curve is $\mathscr{I}_{Cl}$. The state $\hat{B}$ corresponds to the state in the intersection between $\mathscr{R}_\Delta$ and $\mathscr{I}_{Cl}$. The Riemann solution construction is described in Fig. E.14. right *b)- right.* Similar waves. The Riemann solution solution is described in Fig. E.16.

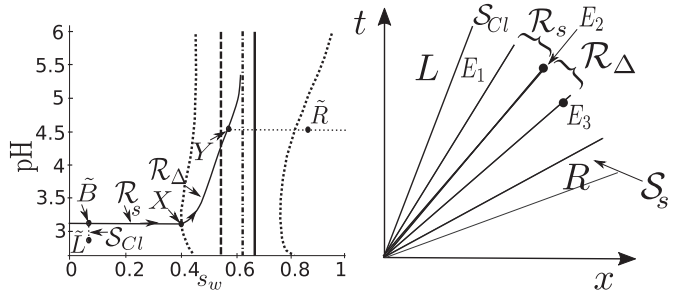

Fig. E.16. *a)- left.* Wave sequence for states satisfying *b)- right.* The Riemann solution described in (4). The Riemann solution in the (x, t)-plane. Here $E_1 = (Sw_L, pH_L, Cl_R)$, $E_1 = (Sw_A, pH_L, Cl_R)$ and $E_3 = (Sw_B, pH_R, Cl_R)$.

quences and we obtain a procedure to solve the complete Riemann problem for states L and R in which waves obey the geometric compatibility condition. Once we have the Riemann solution in the (S_w, pH, Cl) space, we can obtain the solution in the full space (S_w, pH, Cl, u), see Lambert and Marchesin (2009); Lambert et al. (2010).

Obtaining the wave sequence in the (S_w, pH) space, we use the bifurcation curves obtained by the projection on the (S_w, pH) plane of the coincidence

and inflection surfaces described in Appendix D, see Fig. E.13 left. These bifurcation curves divide the physical space (S_w, pH) in the subregions R_1 to R_6 as in Fig. E.13 right. In R_1, we have that $\lambda_{Cl} < \lambda_s < \lambda_\Delta$; in R_2 and R_3, $\lambda_{Cl} < \lambda_\Delta < \lambda_s$; in R_4, $\lambda_\Delta < \lambda_{Cl} < \lambda_s$; in R_5, $\lambda_\Delta < \lambda_s < \lambda_{Cl}$; in R_6, $\lambda_s < \lambda_\Delta < \lambda_{Cl}$.

The geometrical compatibility condition requires the following rule: When a Riemann datum $\tilde{L}$ belongs to the subregions R_2 to R_5 where $\lambda_\Delta < \lambda_s$, we take as initial wave a composition rarefaction shock wave $\mathscr{S}_\Delta$ or $\mathscr{R}_\Delta$, followed by either the constant state or a saturation wave (see below), which can be either of the rarefaction $(\mathscr{R}_s)$ or shock $(\mathscr{S}_s)$ and must have a velocity higher or equal than the previous wave. On the other hand, when $\tilde{L}$ belongs to the subregions R_1 and R_6 $(\lambda_\Delta > \lambda_s)$, we start with a saturation $\mathscr{R}_s$ or shock $\mathscr{S}_s$ wave followed by waves of type S_Δ or $\mathscr{R}_\Delta$. Besides, in subregions R_1 to R_3, $\mathscr{S}_{Cl}$ has the characteristic speed λ_{Cl} slower than the rest of the waves; in R_4, λ_{Cl} is faster than λ_Δ and λ_{Cl} slower than λ_s and in R_5 and R_6 is faster than the speed of the other waves. We utilize these velocities to obtain the Riemann solution.

Taking into account above comments, we show in details how to solve the Riemann problem from the state L to R. We analyze the case in which $R = (Sw_R, pH_R)$ belong to the line $pH = pH_R$, which are shown in Fig. E.14 right and some chosen left L states:

(*III*) When $\tilde{L} = (Sw_L, pH_L)$ is in R_6 and $\tilde{R} = (Sw_R, pH_R)$ is such that $pH_L < pH_R$, the first wave is $\mathscr{R}_s(L)$. This wave is constructed from $\tilde{L}$ to state $A = (Sw_A, pH_A)$ at the coincidence curve $\mathscr{C}_{s\Delta}$, such that $\lambda_s(A, Cl_L) = \lambda_\Delta(A, Cl_L) < \lambda_{Cl}(A, Cl_L)$. From A, we have a rarefaction $\mathscr{R}_\Delta(A)$. From here, we use the projections of the waves in the (Cl, pH) planes, which is useful to leave a state from $Cl = CL_L$ to $Cl = Cl_R$ (see Fig. E.15). We draw this curve to state $B = (Sw_B, pH_B, Cl_B)$ (we remind that $\tilde{B} = (Sw_B, pH_B)$ and $\widehat{B} = (Cl_B, pH_B)$). Notice that this state B is such that its projection in the (Cl, pH) plane, denoted by $\widehat{B}$, lies at the intersection of curve $\mathscr{S}_s$ from $\widehat{R}$ to $\mathscr{R}_\Delta$ from $\widehat{L}$, see Fig. E.15 left. Notice that the coordinate $pH_B > pH_R$. From B, we have five possibilities (III.1), (III.2), (III.3), (III.4) and (III.5), which we describe below:

(*III*.1) We assume $\tilde{R} \in R_5$ (see Fig. E.13) and $Sw_C < Sw_R < Sw_B$, here Sw_C corresponds to a coordinate of state $C = (Sw_C, pH_R)$ on the coincidence surface $\mathscr{C}_{sCl}$. In this case from $\tilde{B}$ to state (Sw_R, pH_B), we have a $\mathscr{R}_s(\tilde{B})$, such that $\lambda_s(Sw_{\tilde{R}}, pH_{\tilde{R}}, Cl_L) < \lambda_{Cl}(Sw_{\tilde{R}}, pH_{\tilde{R}}, Cl_L)$. From (Sw_R, pH_B) we have a wave $\mathscr{S}_{Cl}$ connecting (Sw_R, pH_R, Cl_L) to R, i.e. the Riemann solution consists of $L \underset{\rightarrow}{\overset{\mathscr{R}_s}{}} (Sw_A, pH_A, Cl_L) \underset{\rightarrow}{\overset{\mathscr{R}_\Delta}{}} (Sw_B, pH_B, Cl_L) \underset{\rightarrow}{\overset{\mathscr{R}_s}{}} (Sw_R, pH_B, Cl_L) \underset{\rightarrow}{\overset{\mathscr{S}_{Cl}}{}} R$.

(*III*.2) We assume that $\tilde{R} \in R_4$ (see Fig. E.13) and $Sw_D < Sw_R < Sw_C$, here Sw_D corresponds to a coordinate of state $D = (Sw_D, pH_R)$ on the inflection $\mathscr{I}_s$. In this case, from $\tilde{B}$ to state C we have a $\mathscr{R}_s$ such that $\lambda_s(Sw_C, pH_B, Cl_L) = \lambda_{Cl}(Sw_R, pH_B, Cl_L)$. From C, connecting $C = (Sw_C, pH_B, Cl_L)$ to (Sw_C, pH_R, Cl_R), we have a curve $\mathscr{S}_{Cl}$, with speed λ_{Cl}. In the projected (Sw, pH) plane $Cl = Cl_R$, we continue $\mathscr{R}_s$ from C to $\tilde{R}$. The Riemann solution consists of a sequence of waves, i.e. $L \xrightarrow{\mathscr{R}_s} (Sw_A, pH_A, Cl_L) \xrightarrow{\mathscr{R}_\Delta} (Sw_B, pH_B, Cl_L) \xrightarrow{\mathscr{R}_s} (Sw_C, pH_B, Cl_L) \xrightarrow{\mathscr{S}_{Cl}} (Sw_C, pH_R, Cl_R) \xrightarrow{\mathscr{R}_s} R$.

(*III*.3) We assume $\tilde{R} \in R_2$ or $\tilde{R} \in R_1$ and $Sw_R < Sw_D$. In this case, from $\tilde{B}$ to state C, we have a $\mathscr{R}_s$ such that $\lambda_s(Sw_C, pH_R, Cl_L) = \lambda_{Cl}(Sw_R, pH_R, Cl_L)$. From C, connecting $C = (Sw_C, pH_B, Cl_L)$ to (Sw_C, pH_B, Cl_R), we have a wave $\mathscr{S}_{Cl}$, with speed λ_{Cl}. In the projected (Sw, pH) plane $Cl = Cl_R$, we continue $\mathscr{R}_s$ from C to state $E = (Sw_E, pH_R)$ such that the shock speed from E to $\tilde{R}$, denoted by $\sigma(E, \tilde{R})$, has the same speed as $\lambda_s(E)$, i.e. $\sigma(E, \tilde{R}) = \lambda_s(E, Cl_R)$. Connecting E to $\tilde{R}$, there is a shock $\mathscr{S}_s$. The Riemann solution consists of $L \xrightarrow{\mathscr{R}_s} (Sw_A, pH_A, Cl_L) \xrightarrow{\mathscr{R}_\Delta} (Sw_B, pH_B, Cl_L) \xrightarrow{\mathscr{R}_s} (Sw_C, pH_B, Cl_L) \xrightarrow{\mathscr{S}_{Cl}} (Sw_C, pH_R, Cl_R) \xrightarrow{\mathscr{R}_s} (Sw_E, pH_R, Cl_R) \xrightarrow{\mathscr{R}_s} R$ (Fig. E.14 right).

(*III*.4) We assume that $\tilde{R} \in R_6$ (In Fig. E.14 right), $\tilde{R}$ belongs to the region 5 or 6, but it is given by the condition below). We assume also $Sw_B < Sw_R < Sw_M$, here $M = (Sw_M, pH_M)$ is the state such that $\sigma(Sw_B, Sw_M) = \lambda_{Cl}(Sw_B, pH_B, Cl_L)$. Notice that in the direction of state with saturation coordinate Sw_B to state with saturation coordinate Sw_R we have a $\mathscr{S}_s$, however, the shock speed connecting these two states is larger than λ_{Cl}. Thus we have a wave $\mathscr{S}_{Cl}$, with speed λ_{Cl}, connecting $B = (Sw_B, pH_B, Cl_L)$ to (Sw_B, pH_R, Cl_R). In the projected (Sw, pH) plane, we connect (Sw_B, pH_R) to state $\tilde{R}$ with a shock $\mathscr{S}_s$. The Riemann solution consists of $L \underset{\rightarrow}{\overset{\mathscr{R}_s}{}} (Sw_A, pH_A, Cl_L) \underset{\rightarrow}{\overset{\mathscr{R}_\Delta}{}} (Sw_B, pH_B, Cl_L) \underset{\rightarrow}{\overset{\mathscr{S}_{Cl}}{}} (Sw_B, pH_R, Cl_R) \underset{\rightarrow}{\overset{\mathscr{S}_s}{}} R$.

(*III*.5) We assume $\tilde{R} \in R_6$ (In Fig. E.14 right, $\tilde{R}$ belongs to the region R_5 or R_6, but it is given by the condition below). We assume also $Sw_M < Sw_R < Sw_N$, here $N = (Sw_N, pH_N)$ is the state such that $\sigma(Sw_B, Sw_N) = \lambda_\Delta(Sw_B, pH_B, Cl_L)$, i.e., any shock from a state (Sw_B, pH_B) to state (Sw^*, pH_R) for $Sw^* > Sw_N$ has speed smaller than $\lambda_\Delta(Sw_B, pH_B, Cl_L)$, thus this state cannot be reached by a sequence of this type. Here the shock speed connecting a state with coordinate Sw_B to state with coordinate Sw_R is smaller than λ_{Cl}. Thus from (Sw_B, pH_B) to (Sw_R, pH_B) we have a shock $\mathscr{S}_s$, and finally connecting (Sw_R, pH_B, Cl_L) to (Sw_R, pH_R, Cl_R) a shock $\mathscr{S}_{Cl}$. The Riemann solution consists of $L \underset{\rightarrow}{\overset{\mathscr{R}_s}{}} (Sw_A, pH_A, Cl_L) \underset{\rightarrow}{\overset{\mathscr{R}_\Delta}{}} (Sw_B, pH_B, Cl_L) \underset{\rightarrow}{\overset{\mathscr{S}_s}{}} (Sw_R, pH_B, Cl_L) \underset{\rightarrow}{\overset{\mathscr{S}_{Cl}}{}} R$.

For state R for which coordinate $Sw_R > Sw_N$, we need a different wave sequence, which we do not construct here, but the construction should respect the geometrical compatibility of waves.

To show a possibility for which the first wave is a $\mathscr{S}_{Cl}$, see Fig. E.16, we construct the following wave.

(IV)- If we consider L and R such that $\tilde{L}$ is in R_1 and $\tilde{R}$ is in R_6, we know that the slower wave is λ_{Cl}. Thus the first wave from $\tilde{L}$ is a $\mathscr{S}_{Cl}$ to $B = (Sw_B, pH_B, Cl_R)$. This state B is obtained such that $\widehat{B} = (pH_B, Cl_R)$ lies on the intersection between $\mathscr{S}_{Cl}$ from $\widehat{L}$ and $\mathscr{R}_\Delta$ from $\widehat{R}$ in the (Cl, pH) plane, see Fig. E.15 right. We define the state $\tilde{B} = (Sw_B, pH_B)$ in the (Sw, pH) plane, thus from $\tilde{B}$, connecting $\tilde{B}$ to $X = (Sw_X, pH_B)$ there exists a $\mathscr{R}_s$ which stay on the coincidence curve $\mathscr{C}_{s\Delta}$. From X to a state $Y = (Sw_Y, pH_R)$ there is a rarefaction $\mathscr{R}_\Delta$ and from Y we have a shock $\mathscr{S}_s$ to state $\tilde{R}$. The Riemann solution consists of $L \underset{\rightarrow}{\overset{\mathscr{S}_{Cl}}{}} (Sw_L, pH_B, Cl_R) \underset{\rightarrow}{\overset{\mathscr{R}_s}{}} (Sw_X, pH_B, Cl_R) \underset{\rightarrow}{\overset{\mathscr{R}_\Delta}{}} (Sw_Y, pH_R, Cl_R) \underset{\rightarrow}{\overset{\mathscr{S}_s}{}} R$. In Fig. E.16 left we describe the wave sequence in the projected (Sw, pH) plane and in Fig. E.16 right we describe the solution in (x,t)−plane.

References

Anderson, G.M., Crerar, D.A., 1993. Thermodynamics in Geochemistry: the Equilibrium Model. Oxford University Press on Demand.

Anderson, W.G., et al., 1987. Wettability literature survey part 5: the effects of wettability on relative permeability. J. Pet. Technol. 39 (11), 1–453.

Appelo, C., Parkhurst, D.L., Post, V., 2014. Equations for calculating hydrogeochemical reactions of minerals and gases such as co2 at high pressures and temperatures. Geochimica Cosmochimica Acta 125, 49–67.

Appelo, C., Postma, D., 1999. A consistent model for surface complexation on birnessite (-mno 2) and its application to a column experiment. Geochimica Cosmochimica Acta 63 (19), 3039–3048.

Appelo, C.A.J., Postma, D., 2004. Geochemistry, Groundwater and Pollution. CRC press.

Beyer, R., Staples, B., 1986. Pitzer-Debye-Hückel limiting slopes for water from 0 to 350 c and from saturation to 1 kbar. J. Solut. Chem. 15 (9), 749–764.

Bradley, D.J., Pitzer, K.S., 1979. Thermodynamics of electrolytes. 12. dielectric properties of water and debye-hueckel parameters to 350. degree. c and 1 kbar. J. Phys. Chem. 83 (12), 1599–1603.

Bryant, S., Schechter, R., Lake, L., 1986. Interactions of precipitation/dissolution waves and ion exchange in flow through permeable media. AIChE J. 32 (5), 751–764.
Bryant, S., Schechter, R., Lake, L., 1987. Mineral sequences in precipitation/dissolution waves. AIChE J. 33 (8), 1271–1287.
Buckley, S.E., Leverett, M., et al., 1942. Mechanism of fluid displacement in sands. Trans. AIME 146 (01), 107–116.
Byrne, P.A., Stoessell, R.K., 1982. Methane solubilities in multisalt solutions. Geochimica Cosmochimica Acta 46 (11), 2395–2397.
Chou, G.F., Forbert, R.R., Prausnitz, J.M., 1990. High-pressure vapor-liquid equilibria for carbon dioxide/n-decane, carbon dioxide/tetralin, and carbon dioxide/n-decane/tetralin at 71.1 and 104.4. degree. c. J. Chem. Eng. Data 35 (1), 26–29.
Christensen, R., et al., 1961. Carbonated waterflood results–Texas and Oklahoma. In: Annual Meeting of Rocky Mountain Petroleum Engineers of AIME. Society of Petroleum Engineers.
Clarke, E.C.W., Glew, D.N., 1980. Evaluation of Debye–Hückel limiting slopes for water between 0 and 150 c. J. Chem. Soc. Faraday Trans. 1 Phys. Chem. Condens. Phases 76, 1911–1916.
Cullick, A.S., Mathis, M.L., 1984. Densities and viscosities of mixtures of carbon dioxide and n-decane from 310 to 403 k and 7 to 30 mpa. J. Chem. Eng. Data 29 (4), 393–396.
De Nevers, N., et al., 1964. A calculation method for carbonated water flooding. Soc. Pet. Eng. J. 4 (01), 9–20.
Dong, Y., Dindoruk, B., Ishizawa, C., Lewis, E.J., et al., 2011. An experimental investigation of carbonated water flooding. In: SPE Annual Technical Conference and Exhibition. Society of Petroleum Engineers.
Dumore, J., Hagoort, J., Risseeuw, A., et al., 1984. An analytical model for one-dimensional, three-component condensing and vaporizing gas drives. Soc. Pet. Eng. J. 24 (02), 169–179.
Eustaquio-Rincón, R., Trejo, A., 2001. Solubility of n-octadecane in supercritical carbon dioxide at 310, 313, 333, and 353 k, in the range 10–20 mpa. Fluid phase equilibria 185 (1), 231–239.
Farajzadeh, R., Matsuura, T., van Batenburg, D., Dijk, H., et al., 2012. Detailed modeling of the alkali/surfactant/polymer (asp) process by coupling a multipurpose reservoir simulator to the chemistry package phreeqc. SPE Reserv. Eval. Eng. 15 (04), 423–435.
Fernandez, D., Goodwin, A., Lemmon, E.W., Levelt Sengers, J., Williams, R., 1997. A formulation for the static permittivity of water and steam at temperatures from 238 k to 873 k at pressures up to 1200 mpa, including derivatives and debye–hückel coefficients. J. Phys. Chem. Reference Data 26 (4), 1125–1166.
Glimm, J., 1965. Solutions in the large for nonlinear hyperbolic systems of equations. Commun. pure Appl. Math. 18 (4), 697–715.
Grogan, A., Pinczewski, W., et al., 1987. The role of molecular diffusion processes in tertiary CO_2 flooding. J. Pet. Technol. 39 (05), 591–602.
Helfferich, F.G., 1989. The theory of precipitation/dissolution waves. AIChE J. 35 (1), 75–87.
Helfferich, F.G., et al., 1981. Theory of multicomponent, multiphase displacement in porous media. Soc. Pet. Eng. J. 21 (01), 51–62.
Helmut, W., 2011. Thermal effects in the injection of CO_2 in deep underground aquifer. Doctoral Thesis. IMPA.
Hickok, C., Christensen, R., Ramsay Jr., H., et al., 1960. Progress review of the k&s carbonated waterflood project. J. Pet. Technol. 12 (12), 20–24.
Hirasaki, G., et al., 1996. Dependence of waterflood remaining oil saturation on relative permeability, capillary pressure, and reservoir parameters in mixed-wet turbidite sands. SPE Reserv. Eng. 11 (02), 87–92.
Honarpour, M.M., Koederitz, F., Herbert, A., 1986. Relative Permeability of Petroleum Reservoirs.
Hubbert, M.K., et al., 1956. Darcy's Law and the Field Equations of the Flow of Underground Fluids.
Israelachvili, J.N., 2015. Intermolecular and Surface Forces. Academic press.
Jennings, D.W., Schucker, R.C., 1996. Comparison of high-pressure vapor- liquid equilibria of mixtures of co2 or propane with nonane and c9 alkylbenzenes. J. Chem. Eng. Data 41 (4), 831–838.
Johns, R., Dindoruk, B., Orr Jr., F., et al., 1993. Analytical theory of combined condensing/vaporizing gas drives. SPE Adv. Technol. Ser. 1 (02), 7–16.
Kariznovi, M., Nourozieh, H., Abedi, J., 2013. Phase composition and saturated liquid properties in binary and ternary systems containing carbon dioxide, n-decane, and n-tetradecane. J. Chem. Thermodyn. 57, 189–196.
Kukarni, A.A., Zarah, B.Y., Luks, K.D., Kohn, J.P., 1974. Phase-equilbriums behavior of system carbon dioxide-n-decane at low temperatures. J. Chem. Eng. Data 19 (1), 92–94.
Lake, L.W., 1989. Enhanced Oil Recovery.
Lake, L.W., Johns, R.T., Rossen, W.R., Pope, G.A., 2014. Fundamentals of Enhanced Oil Recovery.
Lambert, W., Marchesin, D., 2009. The Riemann problem for multiphase flows in porous media with mass transfer between phases. J. Hyperbolic Differ. Equations 6 (04), 725–751.
Lambert, W., Marchesin, D., Bruining, J., 2010. The Riemann solution for the injection of steam and nitrogen in a porous medium. Transp. Porous Media 81 (3), 505–526.
Lax, P.D., 1957. Hyperbolic systems of conservation laws ii. Commun. pure Appl. Math. 10 (4), 537–566.
Leverett, M.C., et al., 1939. Flow of oil-water mixtures through unconsolidated sands. Trans. AIME 132 (01), 149–171.
Liu, T.P., 1974. The Riemann problem for general 2× 2 conservation laws. Trans. Am. Math. Soc. 199, 89–112.
Liu, T.-P., 1975. The Riemann problem for general systems of conservation laws. J. Differ. Equations 18 (1), 218–234.
Lorentz, H., 1913. Opmerkingen bij het artikel van dr. .A. H. Borgesius, de ingenieur. De. Ing. 49 (2), 24–26.
Merkel, B.J., Planer-Friedrich, B., Nordstrom, D.K., 2005. Groundwater geochemistry. A Pract. Guide Model. Nat. Contam. Aquatic Syst. 2.
Morrow, N., Buckley, J., et al., 2011. Improved oil recovery by low-salinity waterflooding. J. Pet. Technol. 63 (05), 106–112.
Muskat, M., Meres, M.W., 1936. The flow of heterogeneous fluids through porous media. Physics 7 (9), 346–363.
Nagarajan, N., Robinson Jr., R., 1986. Equilibrium phase compositions, phase densities, and interfacial tensions for carbon dioxide+ hydrocarbon systems. 2. carbon dioxide + n-decane. J. Chem. Eng. Data 31 (2), 168–171.
Oleinik, O.A., 1957. Discontinuous solutions of non-linear differential equations. Uspekhi Mat. Nauk. 12 (3), 3–73.
Orr, F.M., 2007. Theory of Gas Injection Processes. Tie-Line Publications.
Parkhurst, D.L., Appelo, C., 2013. Description of Input and Examples for Phreeqc Version 3: a Computer Program for Speciation, Batch-reaction, One-dimensional Transport, and Inverse Geochemical Calculations. Tech. rep.. US Geological Survey.
Parkhurst, D.L., Appelo, C., et al., 1999. User's Guide to Phreeqc (Version 2): a Computer Program for Speciation, Batch-reaction, One-dimensional Transport, and Inverse Geochemical Calculations.
Pitzer, K.S., 1981. Characteristics of very concentrated aqueous solutions. Phys. Chem. Earth 13, 249–272.
Pitzer, K.S., 1987. A Thermodynamic Model for Aqueous Solutions of Liquid-like Density.
Pitzer, K.S., Mayorga, G., 1973. Thermodynamics of electrolytes. ii. activity and osmotic coefficients for strong electrolytes with one or both ions univalent. J. Phys. Chem. 77 (19), 2300–2308.
Poling, B.E., Prausnitz, J.M., O'connell, J.P., et al., 2001. Prop. gases Liq, 5. Mcgraw-hill, New York.
Pope, G. A. e. a, 1980. The application of fractional flow theory to enhanced oil recovery. Soc. Pet. Eng. J. 20 (03), 191–205.
Ramesh, A., Dixon, T., et al., 1973. Numerical simulation of carbonated waterflooding in a heterogeneous reservoir. In: SPE Symposium on Numerical Simulation of Reservoir Performance. Society of Petroleum Engineers.
Randall, M., Failey, C.F., 1927a. The activity coefficient of gases in aqueous salt solutions. Chem. Rev. 4 (3), 271–284.
Randall, M., Failey, C.F., 1927b. The activity coefficient of non-electrolytes in aqueous salt solutions from solubility measurements. the salting-out order of the ions. Chem. Rev. 4 (3), 285–290.
Randall, M., Failey, C.F., 1927c. The activity coefficient of the undissociated part of weak electrolytes. Chem. Rev. 4 (3), 291–318.
Reamer, H., Sage, B., 1963. Phase equilibria in hydrocarbon systems. volumetric and phase behavior of the n-decane-co2 system. J. Chem. Eng. Data 8 (4), 508–513.
Reardon, E.J., Langmuir, D., 1976. Activity coefficients of mgcoo3 and casoo4 ion pairs as a function of ionic strength. Geochimica Cosmochimica Acta 40 (5), 549–554.
Sander, R., 1999. Compilation of Henry's Law Constants for Inorganic and Organic Species of Potential Importance in Environmental Chemistry.
Scott, J., Forrester, C., et al., 1965. Performance of domes unit carbonated waterflood-first stage. J. Pet. Technol. 17 (12), 1–379.
Shaver, R., Robinson, R., Gasem, K., 2001. An automated apparatus for equilibrium phase compositions, densities, and interfacial tensions: data for carbon dioxide+ decane. Fluid phase equilibria 179 (1), 43–66.
Sohrabi, M., Riazi, M., Jamiolahmady, M., Ireland, S., Brown, C., 2009. Mechanisms of oil recovery by carbonated water injection. In: SCA Annual Meeting.
Welge, H., Johnson, E.F., Ewing Jr., S., Brinkman, F., et al., 1961. The linear displacement of oil from porous media by enriched gas. J. Pet. Technol. 13 (08), 787–796.
Welker, J., et al., 1963. Physical properties of carbonated oils. J. Pet. Technol. 15 (08), 873–876.
Zawisza, A., Malesinska, B., 1981. Solubility of carbon dioxide in liquid water and of water in gaseous carbon dioxide in the range 0.2-5 mpa and at temperatures up to 473 k. J. Chem. Eng. Data 26 (4), 388–391.